



On the Statistics of Baryon Correlation Functions in Lattice QCD

Michael L. Wagman^{1,2} and Martin J. Savage¹
(NPLQCD Collaboration)

¹*Institute for Nuclear Theory, Box 351550, Seattle, WA 98195-1550, USA*

²*Department of Physics, University of Washington, Box 351560, Seattle, WA 98195, USA*

(Dated: September 21, 2022)

A systematic analysis of the structure of single-baryon correlation functions calculated with lattice QCD is performed, with a particular focus on characterizing the structure of the noise associated with quantum fluctuations. The signal-to-noise problem in these correlation functions is shown, as long suspected, to result from a sign problem. The log-magnitude and complex phase are found to be approximately described by normal and wrapped normal distributions respectively. Properties of circular statistics are used to understand the emergence of a late time noise region where standard energy measurements are unreliable. Power-law tails in the distribution of baryon correlation functions, associated with stable distributions and “Lévy flights”, are found to play a central role in their time evolution. A new method of analyzing correlation functions is considered for which the signal-to-noise ratio of energy measurements is constant at late times, rather than degrading exponentially; this permits a reliable extraction of the signal from the noise region. Temporal correlations longer than a specified scale are neglected in this new method, but the resulting systematic bias can be removed via extrapolation. The observations and understanding presented in this work may have significance to other systems exhibiting a sign problem.

I. INTRODUCTION

Modern nuclear physics research relies upon large-scale high-performance computing (HPC) to predict the properties of a diverse array of many-body systems, ranging from the properties of hadrons computed from the dynamics of quarks and gluons, through to the form of gravitational waves emitted from inspiraling binary neutron star systems. In many cases, the entangled quantum nature of these systems and the nonlinear dynamics that define them, preclude analytic calculation of their properties. In these cases, precise numerical evaluations of high-dimensional integrations that systematically approach the quantum path integral are required. Typically, it is average quantities that are determined by Monte Carlo (MC) path integral evaluations. These average values are to be used subsequently in direct comparison with experiment, as input to analytic frameworks with outputs that can then be compared with experiment, or as predictions for critical components of systems that are inaccessible to experiment such as the equation of state of dense matter in explosive astrophysical environments. Enormous amounts of HPC resources are used in such MC calculations to determine average values of quantities and their uncertainties. The central limit theorem, and in particular the $1/\sqrt{N}$ scaling anticipated for the uncertainties associated with average values, are used to make estimates of projected resource requirements. When a system has a “sign problem”, for which the average value of a quantity of interest results from cancellations of (relatively) large contributions, such as found when averaging $e^{i\theta}$, the HPC resources required for accurate numerical estimates of the average(s) are prohibitively large. This is the case for numerical evaluations of the path integrals describing strongly interacting systems with even a modest non-zero net baryon number.

While the quantum fluctuations (noise) of many-body systems contain a wealth of information beyond average values, only a relatively small amount of attention has been paid to refining calculations based upon the structure of the noise. This statement, of course, does not do justice to the fact that all observables (S-matrix elements) in quantum field theory calculations can be determined from vacuum expectation values of products of quantum fields. However, in numerical calculations, it is generally the case that noise is treated as a nuisance, something to reduce as much as needed, as opposed to a feature that may reveal aspects of systems that are obscured through distribution among many expectation values. In the area of Lattice Quantum Chromodynamics (LQCD), which is the numerical technique used to evaluate the quantum path integral associated with Quantum Chromodynamics (QCD) that defines the dynamics of quarks and gluons, limited progress has been made toward understanding the structure of the noise in correlation functions and the physics that it contains.

Strongly interacting quantum systems can be described through path integral representations of correlation functions. In principle, MC evaluation of lattice regularized path integrals can solve QCD as well as many strongly interacting atomic and condensed matter theories. In practice, conceptual obstacles remain and large nuclei and nuclear matter are presently inaccessible to LQCD. In the grand canonical formulation, LQCD calculations with non-zero chemical potential face a sign problem where MC sampling weights are complex and cannot be interpreted as probabilities. In the canonical formulation, calculations with non-zero baryon number face a Signal-to-Noise (StN) problem where statistical uncertainties in MC results grow exponentially at late times. Like the sign problem, the StN problem arises when the sign of a correlation function can fluctuate, at which point cancellations allow for a mean correlation function of much smaller magnitude than a typical MC contribution.

The nucleon provides a relatively simple and well-studied example of a complex correlation function with a StN problem. The zero-momentum Euclidean nucleon correlation function $C(t)$ is guaranteed to have a real mean value by existence of a Hermitian, bounded transfer matrix and the spectral representation

$$\langle C(t) \rangle = \sum_{\mathbf{x}} \langle N(\mathbf{x}, t) \bar{N}(0) \rangle = \sum_{n=0}^{\infty} \tilde{Z}_n Z_n^\dagger e^{-E_n t} \sim e^{-m_N t} \quad , \quad (1)$$

where \bar{N} and N are nucleon creation and annihilation interpolating operators, \tilde{Z}_n^\dagger and Z_n represent the overlap of these interpolating operators onto the n -th QCD eigenstates with quantum numbers of the nucleon, E_n is the energy of the corresponding eigenstate, t is Euclidean time, m_N is the nucleon mass, and throughout this work \sim denotes proportionality in the limit $t \rightarrow \infty$. A phase convention for creation and annihilation operators is assumed so that $C(0)$ is real for all correlation functions in a statistical ensemble. At early times $C(t)$ is approximately real, but at late times it must be treated as a complex quantity. The equilibrium probability distribution for $C(t)$ can be formally defined as

$$\mathcal{P}(C(t)) = Z^{-1} \int \mathcal{D}U e^{-S(U)} \delta(C(t; U) - C(t)) \quad \text{with} \quad Z = \int \mathcal{D}U e^{-S(U)} \quad , \quad (2)$$

where U is a gauge field, $C(U; t)$ is the nucleon correlation function in the presence of a background gauge field U , $\mathcal{D}U$ is the Haar measure for the gauge group, and $S(U)$ is the gauge action arising after all dynamical matter fields have been integrated out. For convenient comparison with LQCD results, a lattice regulator with a lattice spacing equal to unity will be assumed throughout. Unless specified, results will not depend on details of the ultraviolet regulation of $\mathcal{P}(C(t))$.

MC integration of the path integral representation of a partition function, as performed in LQCD calculations, provides a statistical ensemble of background quantum fields. Calculation of $C(U; t)$ in each background field provides a statistical ensemble of correlation functions distributed according to $\mathcal{P}(C(t))$. Understanding the statistical properties of this ensemble is essential for efficient MC calculations, and significant progress has been achieved in this direction since the early days of lattice field theory. Following Parisi [1], Lepage [2] argued that $C(t)$ has a StN problem where the noise, or square root of the variance of $C(t)$, becomes exponentially larger than the signal, or average of $C(t)$, at late times. It is helpful to review the pertinent details of Parisi-Lepage scaling of the StN ratio.

Higher moments of $C(t)$ are themselves field theory correlation functions with well-defined spectral representations.¹ Their late-time behavior is a single decaying exponential whose scale is set by the lowest energy state with appropriate quantum numbers. Assuming that matter fields have been integrated out exactly rather than stochastically, $C(t)^\dagger C(t)$ will contain three valence quarks and three valence antiquarks whose net quark numbers are separately conserved. This does not imply that $|C(t)|^2$ will only contain nucleon-antinucleon states, as nothing prevents these distinct valence quarks and antiquarks from forming lower energy configurations such as three pions. Quadratic moments of the correlation function, therefore, have the asymptotic behavior

$$\langle C(t)^2 \rangle \sim e^{-2m_N t} \quad , \quad \langle |C(t)|^2 \rangle \sim e^{-3m_\pi t} \quad . \quad (3)$$

At late times, the nucleon StN ratio is determined by the slowest-decaying moments at late times, taking the form,

$$\frac{\langle C(t) \rangle}{\sqrt{\langle |C(t)|^2 \rangle}} \sim e^{-(m_N - \frac{3}{2}m_\pi)t} \quad . \quad (4)$$

¹ The n -th moment $\langle C(t)^n \rangle$ represents the n -nucleon nuclear correlation function in the absence of Pauli exchange between quarks in different nucleons. This is formally a correlation function in a partially-quenched theory with nN_f valence quarks and N_f sea quarks. In general, such a theory is guaranteed to have a bounded, but not necessarily Hermitian, transfer matrix [3].

and is therefore exponentially small.² The quantitative behavior of the variance of baryon correlation function in LQCD calculations was investigated in high-statistics studies by the NPLQCD collaboration [7–9] and more recently by Detmold and Endres [10, 11], and was found to be roughly consistent with Parisi-Lepage scaling. One of us [12] extended Parisi-Lepage scaling to higher moments of $C(t)$ and showed that all odd moments of $C(t)$ are exponentially suppressed compared to even moments at late times. Nucleon correlation function distributions are increasingly broad and symmetric with exponentially small StN ratios at late times, as seen, for example, in histograms of the real parts of LQCD correlation functions in Ref. [9].

Beyond moments, the general form of correlation function distributions has also been investigated. Endres, Kaplan, Lee, and Nicholson [13] found that correlation functions in the nonrelativistic quantum field theory describing unitary fermions possess approximately log-normal distributions. They presented general arguments, that are discussed below, suggesting that this behavior might be a generic feature of quantum field theories. Knowledge of the approximate form of the correlation function distribution was exploited to construct an improved estimator, the cumulant expansion, that was productively applied to subsequent studies of unitary fermions [14–17]. Correlation function distributions have been studied analytically in the Nambu-Jona-Lasinio model [18, 19], where it was found that real correlation functions were approximately log-normal but complex correlation functions in a physically equivalent formulation of the theory were broad and symmetric at late times with qualitative similarities to the QCD nucleon distribution. DeGrand [20] observed that meson, baryon, and gauge-field correlation functions in $SU(N_c)$ gauge theories with several choices of N_c are also approximately log-normal at early times where imaginary parts of correlation functions can be neglected. These various observations provide strong empirical evidence that the distributions of real correlation functions in generic quantum field theories are approximately log-normal.

A generalization of the log-normal distribution for complex random variables that approximately describes the QCD nucleon correlation function at late times is presented in this work. To study the logarithm of a complex correlation function, it is useful to introduce the magnitude-phase decomposition

$$C(t) = |C(t)|e^{i\theta(t)} = e^{R(t)+i\theta(t)} \quad . \quad (5)$$

At early times where the imaginary part of $C(t)$ is negligible, previous observations of log-normal correlation functions [20] demonstrate that $R(t)$ is approximately normally distributed. It is shown below that $R(t)$ is approximately normal at all times, and that $\theta(t)$ is approximately normal at early times. Statistical analysis of $\theta(t)$ is complicated by the fact that it is defined modulo 2π . In particular, the sample mean of a phase defined on $-\pi < \theta(t) \leq \pi$ does not necessarily provide a faithful description of the intuitive average phase (consider a symmetric distribution peaked around $\pm\pi$ with a sample mean close to zero). Suitable statistical tools for analyzing $\theta(t)$ are found in the theory of circular statistics and as will be seen below that $\theta(t)$ is described by an approximately wrapped normal distribution.³ This work is based on a high-statistics analysis of 500,000 nucleon correlation functions generated on a single ensemble of gauge-field configurations by the NPLQCD collaboration [24] with LQCD. This ensemble has a pion mass of $m_\pi \sim 450$ MeV, physical strange quark mass, lattice spacing ~ 0.12 fm, and spacetime volume $32^3 \times 96$. The Lüscher-Weisz gauge action [25] and $N_f = 2 + 1$ clover-improved Wilson quark actions [26] were used to generate these ensembles, details of which can be found in Ref. [24]. Exploratory data analysis of this high-statistics ensemble plays a central role below.

Sec. II discusses standard statistical analysis methods in LQCD that introduce concepts used below. In Section III, the magnitude-phase decomposition of the nucleon correlation function and connections to the StN problem are discussed. Section III A describes the distributions of the log-magnitude and its time derivative in more detail, while Section III B describes the distribution of the complex phase and its time derivative and explains how their features lead to systematic bias in standard estimators during a late-time region that is dominated by noise. Section IV draws on these observations to propose an estimator for the nucleon mass in which this systematic bias can be controlled and the associated statistical uncertainties are constant at late times instead of exponentially increasing. Section V conjectures about applications to the spectra of generic complex correlation functions and concludes.

² A generalization of the Weingarten-Witten QCD mass inequalities [4, 5] by Detmold [6] proves that $m_N \geq \frac{3}{2}m_\pi$. Assuming that interaction energy shifts in the three-pion states contributing to the variance correlation function are negligible, the nucleon StN ratio is therefore exponentially small for all quark masses.

³ See Refs. [21–23] for textbook introductions to circular statistics.

II. RELEVANT ASPECTS OF STANDARD ANALYSIS METHODS OF CORRELATION FUNCTIONS

Typically, in calculations of meson and baryon masses and their interactions, correlation functions are generated from combinations of quark- and gluon-level sources and sinks with the appropriate hadron-level quantum numbers. Linear combinations of these correlation functions are formed, either using Variational-Method type techniques [27], or Matrix-Prony [7], or other less automated methods, in order to optimize overlap onto the lowest lying states in the spectrum and establish extended plateaus in relevant effective mass plots (EMPs). In the limit of an infinite number of independent measurements, the expectation value of the correlation function is a real number at all times, and the imaginary part can be discarded as it is known to average to zero. The late time behavior of such correlation functions becomes a single exponential (for an infinite time-direction) with an argument determined by the ground-state energy associated with the particular quantum numbers, or more generally the energy of the lowest-lying state with non-negligible overlap.

The structure of the source and sink play a crucial role in determining the utility of sets of correlation functions. For many observables of interest, it is desirable to optimize the overlap onto the ground state of the system, and to minimize the overlap onto the correlation function dictating the variance of the ground state. In the case of the single nucleon, the sources and sinks, \mathcal{O} , are tuned in an effort to have maximal overlap onto the ground-state nucleon, while minimizing overlap of $\mathcal{O}\mathcal{O}^\dagger$ onto the three-pion ground state [10]. NPLQCD uses momentum projected hadronic blocks generated from quark propagators originating from localized smeared sources to suppress the overlap into the three-pion ground state by a factor of $1/\sqrt{V}$ where V is the lattice volume, e.g. Ref. [7]. For such constructions, the variance of the average scales as $\sim e^{-3m_\pi t}/(VN)$ at large times, where N is the number of statistically independent correlation functions, while the nucleon correlation function scales as $\sim e^{-M_N t}$. For this set up, the StN ratio scales as $\sim \sqrt{VN}e^{-(M_N-3m_\pi/2)t}$, from which it is clear that exponentially large numbers of correlation functions or volumes are required to overcome the StN problem at large times. However, the situation is quite different at short and intermediate times in which the variance correlation function is dominated, not by the three-pion ground state, but by the nucleon-antinucleon excited state, which provides a variance contribution that scales as $\sim e^{-2m_N t}/N$. There is a time interval where the StN ratio is not degrading exponentially, and it is in this interval, which has been dubbed the “Golden Window” [7], where calculations of the lowest-lying states of the nucleon and light nuclei have been performed. The variance in this time interval is generated, in part, by the distribution of overlaps of the source and sink onto the ground state, that differs at each lattice site due to variations in the gluon fields.

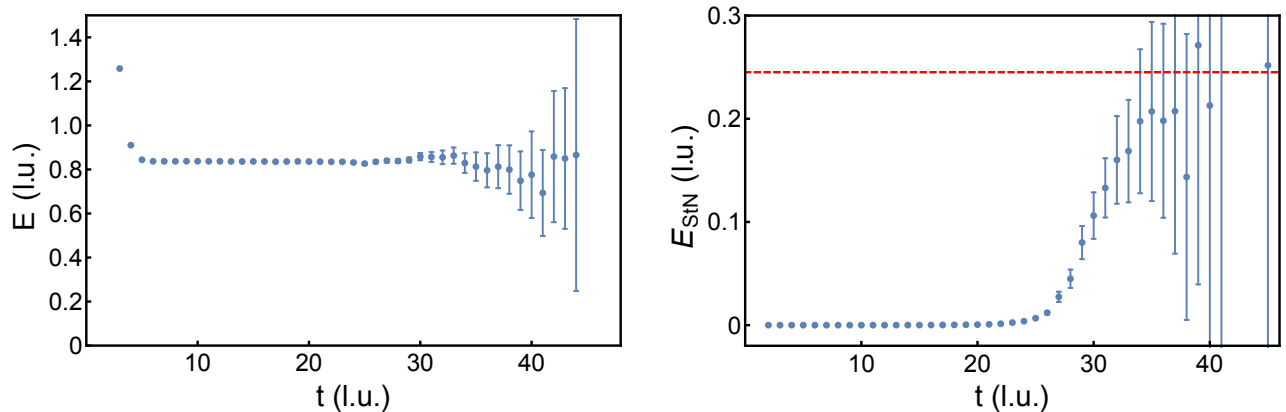


FIG. 1: The EMP associated with the Ξ -baryon correlation function with $\Delta t = 2$ (left panel) and the energy scale associated with the standard deviation of the ground state energy (right panel). This correlation function is a tuned linear combination of those resulting from localized smeared and point sinks and from a localized smeared source at a pion mass of $m_\pi \sim 450$ MeV calculated from 96 sources per configuration on 3538 statistically independent isotropic clover gauge-field configurations [24]. They have been blocked together to form 100 independent samplings of the combined correlation function. The red dashed line in the right panel corresponds to the lowest energy contributing to the StN ratio that is expected to dominate at large times.

EMPs, such as that associated with the Ξ -baryon shown in Fig. 1, are formed from ratios of correlation functions, which become constant when only a single exponential is contributing to the correlation function,

$$\ln \left[\frac{\langle C_i(t) \rangle}{\langle C_i(t + \delta t) \rangle} \right] \rightarrow E_i \delta t \quad , \quad (6)$$

where E_i is the ground state energy in the channel with quantum numbers denoted by “ i ”, and $\langle C_i(t) \rangle$ is the average of the correlation function at time t away from the source. The average is over correlation functions derived from

multiple source points on multiple gauge-field configurations. This is well-known technology and is a “workhorse” in the analysis of LQCD calculations. Typically, δt corresponds to one temporal lattice spacing, and the jackknife and bootstrap resampling techniques are used to generate covariance matrices in the plateau interval used to extract the ground-state energy from a correlated χ^2 -minimization [8, 9, 28].⁴ The energy can be extracted from an exponential fit to the correlation function or by a direct fit to the effective mass itself. Because correlation functions generated from the same, and nearby, gauge-field configuration are correlated, typically they are blocked to form one average correlation function per configuration, and blocked further over multiple configurations, to create an smaller ensemble containing (approximately) statistically independent samplings of the correlation function.

It is known that baryon correlation functions contain outliers over $\sim m_\pi^{-1}$ time scales, as shown in the Fig. 2, which contribute significantly to off-diagonal elements in covariance matrices generated from averages through either jackknife or bootstrap resampling. As δt is increased beyond $\sim m_\pi^{-1}$, covariance matrices become increasingly diagonal

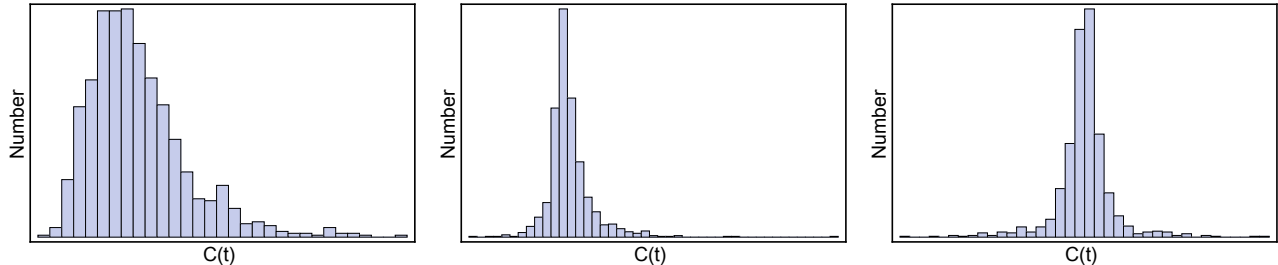


FIG. 2: The distribution of the real part of 10^3 nucleon correlation functions at time slices $t = 6$ (left panel), $t = 16$ (middle panel) and $t = 24$ (right panel).

as the values of correlation functions on separated time slices become de-correlated, as shown in Fig. 3. The utility of

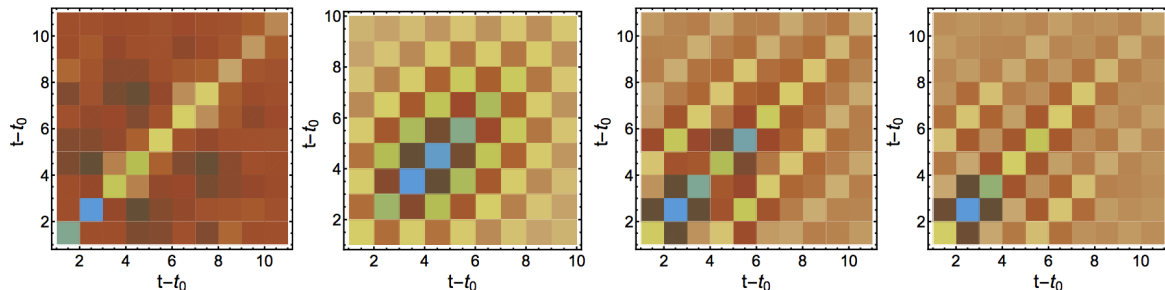


FIG. 3: The inverse covariance matrix in the plateau region of the Ξ -baryon EMP, starting at time-slice t_0 , for $\delta t = 1, 2, 3, 4$ (from left to right). The correlation function is the same as that described in the caption of Fig. 1. In each case, a plateau length of 10 time-slices results in an acceptable value of χ^2/dof from a correlated fit. The matrix was determined using Jackknife resampling with the average of sampled functions to determine each element.

robust estimators, such as the median and the Hodges-Lehmann estimator, with reduced sensitivity to outliers, has been explored in Ref. [9]. When the median and average of a function are known to coincide, there are advantages to using the median or Hodges-Lehmann estimator to determine the average of a distribution. The associated uncertainty can be estimated with the “median absolute deviation” (MAD), and be related to the standard deviation with a well-known scaling factor. The inverse covariance matrix associated with the Hodges-Lehmann estimator is shown in Fig. 4. Importantly, it has been shown by David Kaplan, using a set of NPLQCD baryon correlation functions, that the distribution of late time correlation functions is consistent with a stable distribution [32].

⁴ For pedagogical introductions to LQCD uncertainty quantification with resampling methods, see Refs. [9, 29–31].

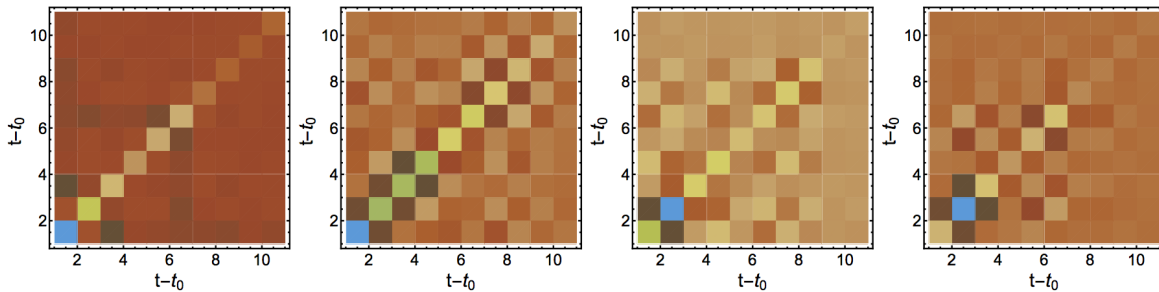


FIG. 4: The inverse covariance matrix in the plateau region of the Ξ -baryon EMP, starting at time-slice t_0 , for $\delta t = 1, 2, 3, 4$ (from left to right). The correlation function is the same as that described in the caption of Fig. 1. In each case, a plateau length of 10 time-slices results in an acceptable value of χ^2/dof from a correlated fit. The matrix was determined with the Hodges-Lehmann estimator and the median.

III. A MAGNITUDE-PHASE DECOMPOSITION

In terms of the log-magnitude and phase, the mean nucleon correlation functions is

$$\langle C(t) \rangle = \int \mathcal{D}C \mathcal{P}(C(t)) e^{R(t)+i\theta(t)} . \quad (7)$$

In principle, $e^{R(t)}$ could be included in the MC probability distribution used for importance sampling. With this approach, $R(t)$ would contribute as an additional term in a new effective action. The presence of non-zero $\theta(t)$ demonstrates that this effective action would have an imaginary part. The resulting weight therefore could not be interpreted as a probability and importance sampling could not proceed; importance sampling of $C(t)$ faces a sign problem. In either the canonical or grand canonical approach, one-baryon correlation functions are described by complex correlation functions that cannot be directly importance sampled without a sign problem, but it is formally permissible to importance sample according to the vacuum probability distribution, calculate the phase resulting from the imaginary effective action on each background field configuration produced in this way, and average the results on an ensemble of background fields. This approach, known as reweighting, has a long history in grand canonical ensemble calculations but has been generically unsuccessful because statistical averaging is impeded by large fluctuations in the complex phase that grow exponentially with increasing spacetime volume [33–35]. Canonical ensemble nucleon calculations averaging $C(t)$ over background fields importance sampled with respect to the vacuum probability distribution are in effect solving the sign problem associated with non-zero $\theta(t)$ by reweighting. As emphasized by Ref. [18], similar chiral physics is responsible for the exponentially hard StN problem appearing in canonical calculations and exponentially large fluctuations of the complex phase in grand canonical calculations.

Reweighting a pure phase causing a sign problem generically produces a StN problem in theories with a mass gap. Suppose $\langle e^{i\theta(t)} \rangle \sim e^{-m_\theta t}$ for some $m_\theta \neq 0$. Then because $|e^{i\theta(t)}|^2 = 1$ by construction, $\theta(t)$ has the StN ratio

$$\frac{\langle e^{i\theta(t)} \rangle}{\sqrt{\langle |e^{i\theta(t)}|^2 \rangle}} = \langle e^{i\theta(t)} \rangle \sim e^{-m_\theta t} , \quad (8)$$

which is necessarily exponentially small at late times. Non-zero m_θ guarantees that statistical sampling of $e^{i\theta(t)}$ has a StN problem. Strictly, this argument applies to a pure phase but not to a generic complex observable such as $C(t)$ which might receive zero effective mass contribution from $\theta(t)$ and could have important correlations between $R(t)$ and $\theta(t)$. MC LQCD studies are needed to understand whether the pure phase StN problem of Eq. (8) captures some or all of the nucleon StN problem of Eq. (4).

To determine the late-time behavior of correlation functions, it is useful to consider the effective-mass estimator commonly used in LQCD spectroscopy, a special case of eq. (6),

$$m(t) = \ln \left[\frac{\langle C(t) \rangle}{\langle C(t+1) \rangle} \right] . \quad (9)$$

As $t \rightarrow \infty$, the average correlation function can be described by a single exponential whose decay rate is set by the ground state energy, and therefore $m(t) \rightarrow m_N$. The uncertainties associated with $m(t)$ can be estimated by

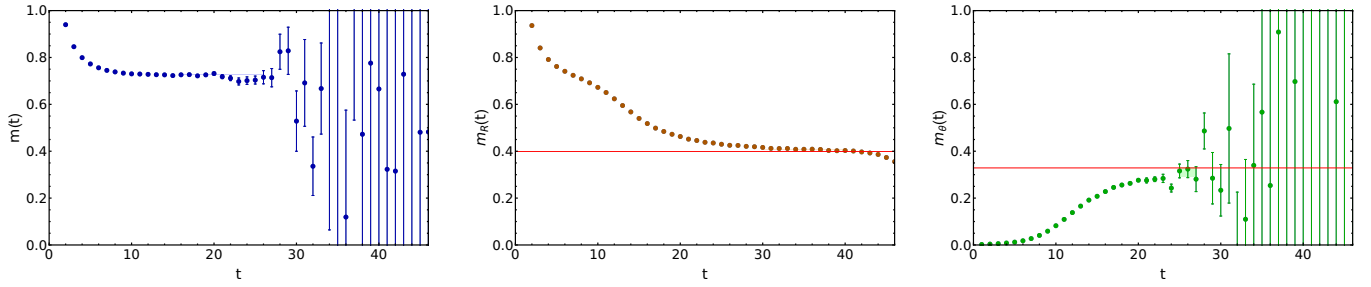


FIG. 5: The left panel shows the nucleon effective mass $m(t)$ as a function of Euclidean time in lattice units. The middle and right panels show the effective masses $m_R(t)$ and $m_\theta(t)$ of the magnitude and phase respectively. Late-time values of $m(t)$, $m_R(t)$, and $m_\theta(t)$ are calculated from constant fits to the shaded plateau regions shown. The asymptotic values of $m_R(t)$ and $m_\theta(t)$ are close to $\frac{3}{2}m_\pi$ and $m_N - \frac{3}{2}m_\pi$ respectively, whose values are indicated for comparison with horizontal red lines. The uncertainties are calculated using bootstrap methods.

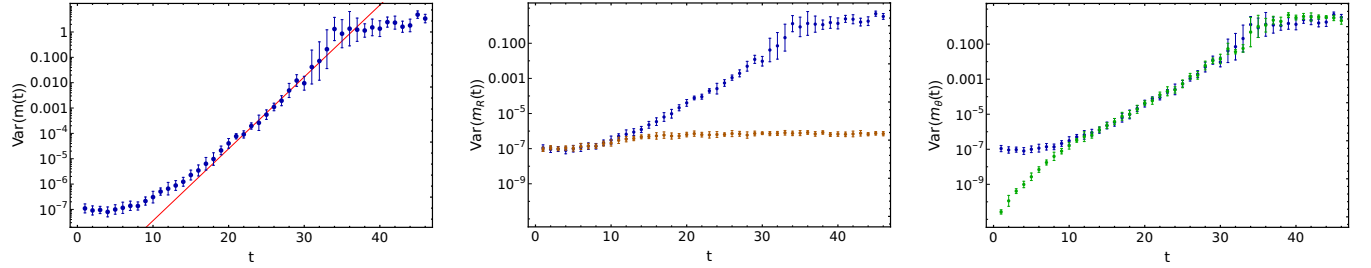


FIG. 6: Variances of the effective mass estimates shown in Fig. 5. The blue points common to all panels show the variance of $m(t)$. The red line in the left plot shows a fit to $e^{2(m_N - \frac{3}{2}m_\pi)t}$ variance growth, where the normalization has been fixed to reproduce the observed variance at $t = 22$. The orange points in the middle panel show the variance of $m_R(t)$. The green points in the right panel show the variance of $m_\theta(t)$.

resampling methods such as bootstrap. The variance of $m(t)$ is generically smaller than that of $\ln \langle C(t) \rangle$ due to cancellations arising from correlations between $\ln [\langle C(t) \rangle]$ and $\ln [\langle C(t+1) \rangle]$ across bootstrap ensembles. Assuming that these correlations do not affect the asymptotic scaling of the variance of $m(t)$, propagation of uncertainties for bootstrap estimates of the variance of $\ln [\langle C(t) \rangle]$ shows that the variance of $m(t)$ scales as

$$\text{Var}(m(t)) \sim \frac{\text{Var}(C(t))}{\langle C(t) \rangle^2} \sim e^{2(m_N - \frac{3}{2}m_\pi)t} \quad . \quad (10)$$

An analogous effective-mass estimator for the late-time exponential decay of the magnitude is

$$m_R(t) = \ln \left[\frac{\langle e^{R(t)} \rangle}{\langle e^{R(t+1)} \rangle} \right] \quad , \quad (11)$$

and an effective-mass estimator for the phase is

$$m_\theta(t) = \ln \left[\frac{\langle e^{i\theta(t)} \rangle}{\langle e^{i\theta(t+1)} \rangle} \right] = \ln \left[\frac{\langle \cos(\theta(t)) \rangle}{\langle \cos(\theta(t+1)) \rangle} \right] \quad , \quad (12)$$

where the reality of the average correlation function has been used.

Figure 5 shows EMPs for $m(t)$, $m_R(t)$, and $m_\theta(t)$ calculated from the LQCD ensemble described previously. The mass of the nucleon, determined from a constant fit in the shaded plateau region $15 \leq t \leq 25$ indicated in Fig. 5, is found to be $m_N = 0.7253(11)(22)$, in agreement with the mass obtained from the golden window in previous studies [24] of $m_N = 0.72546(47)(31)$. $m_R(t)$ and $m_\theta(t)$ do not visually plateau until much later times. For the magnitude, a constant fit in the shaded region $30 \leq t \leq 40$ gives an effective mass $m_R(t) \rightarrow m_R = 0.4085(2)(13)$ which is close to the value $\frac{3}{2}m_\pi = 0.39911(35)(14)$ [24] indicated by the red line. For the phase, a constant fit to the shaded region $25 \leq t \leq 29$ gives an effective mass $m_\theta(t) \rightarrow m_\theta = 0.296(20)(12)$, which is consistent with the value $m_N - \frac{3}{2}m_\pi = 0.32636(58)(34)$ [24] indicated by the red line. It is unlikely that the phase has reached its asymptotic

value by this time, but a signal cannot be established at later times. For $t \geq 30$, large fluctuations lead to complex effective mass estimates for $m(t)$ and $m_\theta(t)$ and unreliable estimates and uncertainties. $m_R(t) + m_\theta(t)$ agrees with $m(t)$ up to $\lesssim 5\%$ corrections at all times, demonstrating that the magnitude and cosine of the complex phase are approximately uncorrelated at the few percent level. This suggests the asymptotic scaling of the nucleon correlation function can be approximately decomposed as

$$\langle C(t) \rangle \approx \langle e^{R(t)} \rangle \langle e^{i\theta(t)} \rangle \sim \left(e^{-\frac{3}{2}m_\pi t} \right) \left(e^{-(m_N - \frac{3}{2}m_\pi)t} \right) \quad (13)$$

For early times $t \lesssim 10$, the means and variances of $m(t)$ and $m_R(t)$ agree up to a small contribution from $m_\theta(t)$. This indicates that the real part of the correlation function is nearly equal to its magnitude at early times. At intermediate times $10 \lesssim t \lesssim 25$, the contribution of $m_\theta(t)$ grows relative to $m_R(t)$, and for $t \gtrsim 15$ the variance of the full effective mass is nearly saturated by the variance of $m_\theta(t)$, as shown in Fig. 6. At intermediate times a linear fit normalized to $\text{Var}(m(t=22))$ with slope $e^{2(m_N - \frac{3}{2}m_\pi)t}$ provides an excellent fit to bootstrap estimates of $\text{Var}(m(t))$, in agreement with the scaling of Eq. (10). $\text{Var}(m_\theta(t))$ is indistinguishable from $\text{Var}(m(t))$ in this region, and $m_\theta(t)$ has an identical StN problem. $\text{Var}(m_R(t))$ has much more mild time variation, and $m_R(t)$ can be reliably estimated at all times without almost no StN problem. At intermediate times, the presence of non-zero $\theta(t)$ signaling a sign problem in importance sampling of $C(t)$ appears responsible for the entire nucleon StN problem.

$m(t)$ approaches its asymptotic value much sooner than $m_R(t)$ or $m_\theta(t)$. This indicates that the overlap of $\bar{N}(0)N(0)$ onto the three-pion ground state in the variance correlation function is greatly suppressed compared to the overlap of $\bar{N}(0)$ onto the one-nucleon signal ground state. Optimization of the interpolating operators for high signal overlap contributes to this. Another contribution arises from momentum projection, which suppresses the variance overlap factor by $\sim 1/(m_\pi^3 V)$ [36]. A large hierarchy between the signal and noise overlap factors provides a golden window visible at intermediate times $10 \lesssim t \lesssim 25$. In the golden window, $m(t)$ approaches its asymptotic value but $\text{Var}(m(t))$ begins to grow exponentially and $m_\theta(t)$ is suppressed compared to $m_R(t)$. Reliable extractions of $m(t)$ are possible in the golden window.

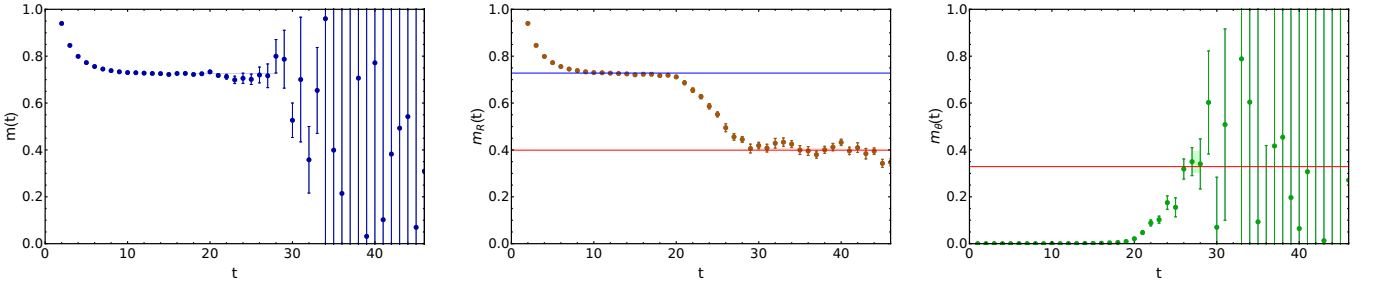


FIG. 7: EMPs from an ensemble of 500 blocked correlation functions, each of which is equal to the sample mean of 1000 nucleon correlation functions. The left panel shows the effective mass $m(t)$ of the blocked correlation functions. The middle panel shows the magnitude contribution $m_R(t)$ and, for reference, a red line at $\frac{3}{2}m_\pi$ and a blue line at m_N are shown. The right panel shows the phase mass $m_\theta(t)$ of the blocked correlation functions along with a red line at $m_N - \frac{3}{2}m_\pi$.

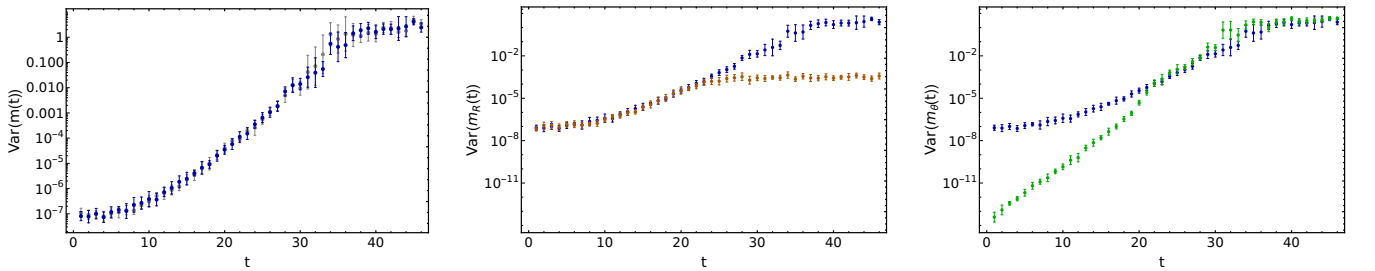


FIG. 8: Bootstrap estimates of the variance of the effective mass using blocked correlation functions. The left panel shows the variance of $m(t)$ for blocked data in blue and the almost indistinguishable variance of $m(t)$ for unblocked data in gray. The middle panel shows the variance of blocked estimates of $m_R(t)$ in orange and the right panel shows the variance of blocked estimates of $m_\theta(t)$ in green.

The effects of blocking, that is averaging subsets of correlation functions and analyzing the distribution of the averages, are shown in Fig. 7. $m_\theta(t)$ is suppressed compared to $m_R(t)$ for longer times in the blocked ensemble, and

the log-magnitude saturates the average and variance of $m(t)$ through intermediate times $t \lesssim 25$. Blocking does not actually reduce the total variance of $m(t)$. Variance in $m(t)$ is merely shifted from the phase to the log-magnitude at intermediate times. This is reasonable, since the imaginary part of $C(t)$ vanishes on average and so blocked correlation functions will have smaller imaginary parts. Still, blocking does not affect $\langle C(t) \rangle$ and only affects bootstrap estimates of $\text{Var}(m(t))$ at the level of correlations between correlation functions in the ensemble. Blocking also does not delay the onset of a late-time noise region $t \gtrsim 35$ where $m(t)$ and $m_\theta(t)$ cannot be reliably estimated.

Eventually the scaling of $\text{Var}(m(t))$ begins to deviate from Eq. (10), and in the noise region $t \gtrsim 35$ the observed variance remains approximately constant (up to large fluctuations). This is inconsistent with Parisi-Lepage scaling. While the onset of the noise region is close to the mid-point of the time direction $t = 48$, a qualitatively similar onset occurs at earlier times in smaller statistical ensembles. Standard statistical estimators therefore do not reproduce the scaling required by basic principles of quantum field theory in the noise region. This suggests systematic deficiencies leading to unreliable results for standard statistical estimation of correlation functions in this region. Systematic deficiencies of standard estimators for baryon and multi-baryon systems have been observed by other groups, see Ref. [37] for a recent critical discussion. These deficiencies may be related to performing fits in the noise region or to performing fits of correlation functions that have not approached their asymptotic plateaus before the onset of the noise region. The emergence of a noise region where standard statistical tools are unreliable can be understood in terms of the circular statistics describing $\theta(t)$ and is explained in Sec. III B. A more straightforward analysis of the distribution of $R(t)$ is first presented below.

A. The Magnitude

Histograms of the nucleon log-magnitude are shown in Fig. 9. Particularly at late times, the distribution of $R(t)$ is approximately described by a normal distribution. Fits to a normal distribution are qualitatively good but not exact, and deviations between normal distribution fits and $R(t)$ data are visible in Fig. 9. Cumulants of $R(t)$ can be used to

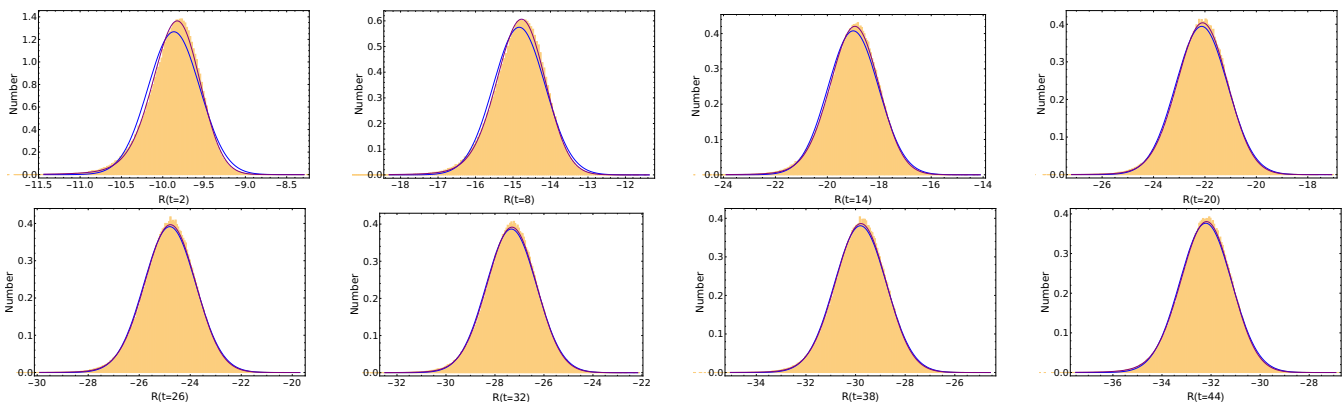


FIG. 9: Normalized histograms of $R(t)$ derived from the LQCD results. The blue curves correspond to best fit normal distributions determined from the sample mean and variance, while the purple curves correspond to maximum likelihood fits to generic stable distributions. See the main text for more details.

quantify these deviations, which can be recursively calculated from its moments by

$$\kappa_n(R(t)) = \langle R(t)^n \rangle - \sum_{m=1}^{n-1} \binom{n-1}{m-1} \kappa_m(R(t)) \langle R(t)^{n-m} \rangle \quad . \quad (14)$$

The first four cumulants of a probability distribution characterize its mean, variance, skewness, and kurtosis respectively. If $C(t)$ were exactly log-normal, the first and second cumulants of $R(t)$, its mean and variance, would fully describe the distribution. Third and higher cumulants of $R(t)$ would all vanish for exactly log-normal $C(t)$. Fig. 10 shows the first four cumulants of $R(t)$. Estimates of higher cumulants of $R(t)$ become successively noisier.

The cumulant expansion of Ref. [13] relates the effective mass of a correlation function to the cumulants of the logarithm of the correlation function. The derivation of Ref. [13] is directly applicable to $m_R(t)$. The characteristic function $\Phi_{R(t)}(k)$, defined as the Fourier transform of the probability distribution function of $R(t)$, can be described

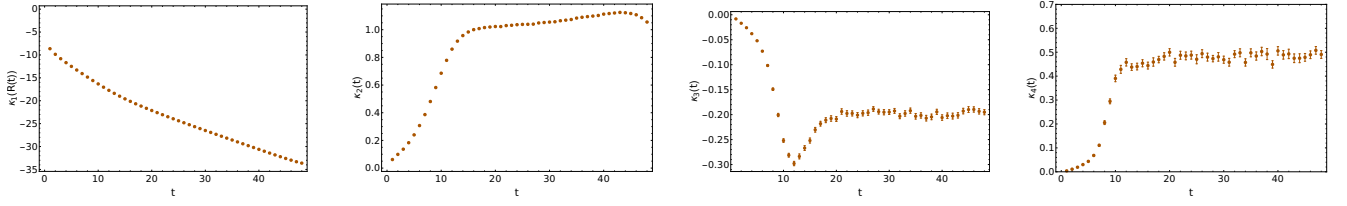


FIG. 10: The first four cumulants of $R(t)$ as functions of t . Cumulants are calculated from sample moments using Eq. (14) and the associated uncertainties are estimated by bootstrap methods. From left to right, the panels show the cumulants $\kappa_1(R(t))$ (mean), $\kappa_2(R(t))$ (variance), $\kappa_3(R(t))$ (characterizing skewness) and κ_4 (characterizing kurtosis).

by a Taylor series for $\ln[\Phi_{R(t)}(k)]$ whose coefficients are precisely the cumulants of $R(t)$,

$$\Phi_{R(t)}(k) = \langle e^{ikR(t)} \rangle = \exp \left[\sum_{n=1}^{\infty} \frac{(ik)^n}{n!} \kappa_n(R(t)) \right]. \quad (15)$$

The average magnitude of $C(t)$ is given in terms of this characteristic function by

$$\langle e^{R(t)} \rangle = \Phi_{R(t)}(-i) = \exp \left[\sum_{n=1}^{\infty} \frac{\kappa_n(R(t))}{n!} \right]. \quad (16)$$

This allows application of the cumulant expansion in Ref. [13] to the effective mass in Eq. (11) to give,

$$m_R(t) = \sum_{n=1}^{\infty} \frac{1}{n!} [\kappa_n(R(t)) - \kappa_n(R(t+1))]. \quad (17)$$

Since $\kappa_n(R(t))$ with $n > 2$ vanishes for normally distributed $R(t)$, the cumulant expansion provides a rapidly convergent series for correlation functions that are close to, but not exactly, log-normally distributed. Note that the right-hand-side of Eq. (17) is simply a discrete approximation suitable for a lattice regularized theory of the time derivative of the cumulants.

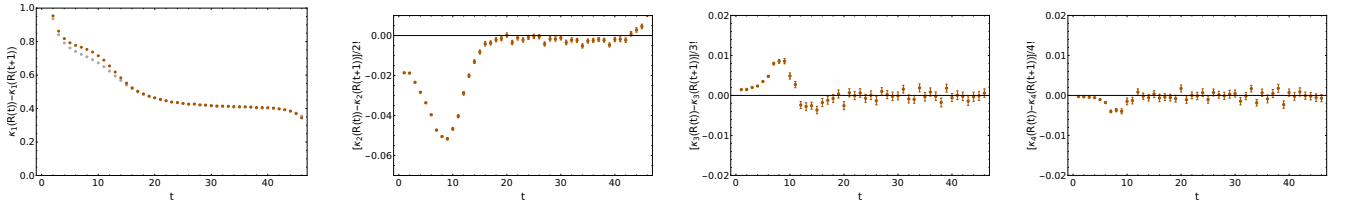


FIG. 11: Contributions to $m_R(t)$ from the first four terms in the cumulant expansion of Ref. [13] given in Eq. (17). In the leftmost panel, the gray points correspond to the unapproximated estimate for $m_R(t)$ (that are also shown in Fig. 5), while the orange points show the contribution from the mean $\kappa_1(R(t))$. The other panels show the contributions to Eq. (17) associated with the variance $\kappa_2(R(t))$, skewness $\kappa_3(R(t))$, and kurtosis $\kappa_4(R(t))$, respectively.

Results for the effective mass contributions of the first few terms in the cumulant expansion of Eq. (17) are shown in Fig. 11. The contribution $\kappa_1(R(t)) - \kappa_1(R(t+1))$, representing the time derivative of the mean, provides an excellent approximation to $m_R(t)$ after early times. $(\kappa_2(R(t)) - \kappa_2(R(t+1)))/2$ provides a very small negative contribution to $m_R(t)$, and contributions from $\kappa_3(R(t))$ and $\kappa_4(R(t))$ are statistically consistent with zero. As $m_R(t)$ approaches its asymptotic value, the log-magnitude distribution can be described to high-accuracy by a nearly normal distribution with very slowly increasing variance and small, approximately constant $\kappa_{3,4}$. The slow increase of the variance of $R(t)$ is consistent with observations above that $|C(t)|$ has no severe StN problem. It is also consistent with expectations that $|C(t)|^2$ describes a (partially-quenched) three-pion correlation function with a very mild StN problem, with a scale set by the attractive isoscalar pion interaction energy.

As Eq. (17) relates $m_R(t)$ to time derivatives of moments of $R(t)$, it is interesting to consider the distribution of the time derivative $\frac{dR}{dt}$. Defining generic finite differences,

$$\Delta R(t, \Delta t) = R(t) - R(t - \Delta t) \quad , \quad (18)$$

the time derivative of lattice regularized results can be defined as the finite difference,

$$\frac{dR}{dt} = \Delta R(t, 1) \quad . \quad (19)$$

If $R(t)$ and $R(t-1)$ were statistically independent, it would be straightforward to extract the time derivatives of the moments of $R(t)$ from the moments of $\frac{dR}{dt}$. The presence of correlations in time, arising from non-trivial QCD dynamics, obstructs a naive extraction of $m_R(t)$ from moments of $\frac{dR}{dt}$. For instance, without knowledge of $\langle R(t)R(t-1) \rangle$ it is impossible to extract the time derivative of the variance of $R(t)$ from the variance of $\frac{dR}{dt}$. While the time derivative of the mean of $R(t)$ is simply the mean of $\frac{dR}{dt}$, time derivatives of the higher cumulants of $R(t)$ cannot be extracted from the cumulants of $\frac{dR}{dt}$ without knowledge of dynamical correlations.

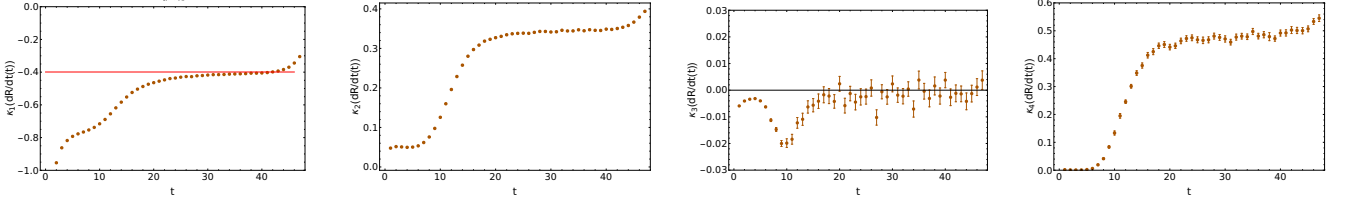


FIG. 12: The first four cumulants of $\frac{dR}{dt}$, determined analogously to the cumulants in Fig. 10.

The cumulants of $\frac{dR}{dt}$ are shown in Fig. 12. As expected, the mean of $\frac{dR}{dt}$ approaches $\frac{3}{2}m_\pi$ at late times. The variance of $\frac{dR}{dt}$ is tending to a plateau which is approximately one-third of the variance of $R(t)$. This implies there are correlations between $R(t)$ and $R(t-1)$ that are on the same order of the individual variances of $R(t)$ and $R(t-1)$. This is not surprising, given that the QCD correlation length is larger than the lattice spacing. No statistically significant κ_3 is seen for $\frac{dR}{dt}$ at late times, but a statistically significant positive κ_4 is found. Normal distribution fits to $\frac{dR}{dt}$ are found to be poor, as shown in Fig. 13, as they underestimate both the peak probability and the probability of finding “outliers” in the tails of the distribution. Interestingly, Fig. 12, and histograms of $\frac{dR}{dt}$ shown in Fig. 13, suggest that the distribution of $\frac{dR}{dt}$ becomes approximately time-independent at late times.

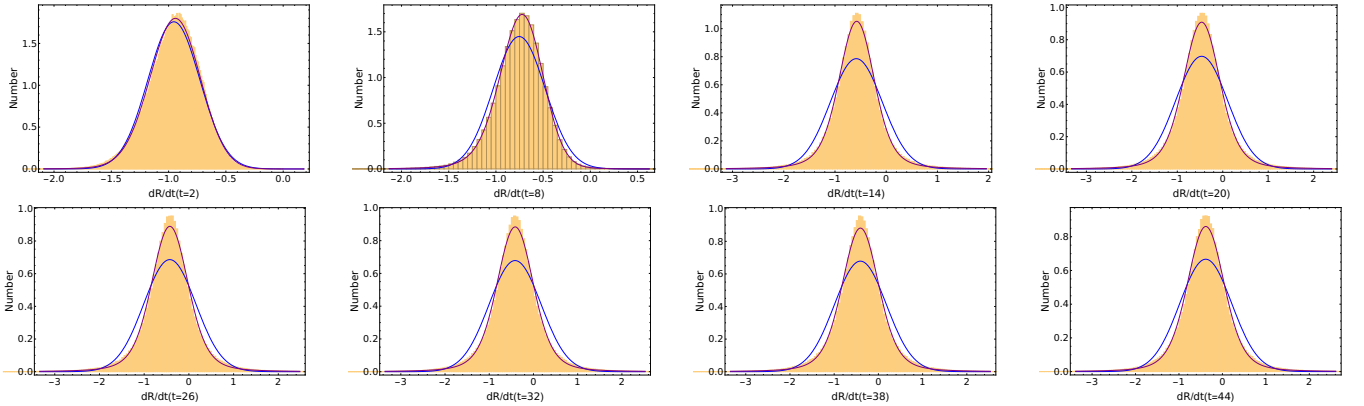


FIG. 13: Histograms of $\frac{dR}{dt}$, defined as the finite difference $\Delta R(t, 1)$ given in Eq. (18). The blue curves in each panel correspond to the best-fit normal distribution, while the purple curves correspond to the best-fit stable distribution.

Stable distributions are found to provide a much better description of $\frac{dR}{dt}$, and are consistent with the heuristic arguments for log-normal correlation functions given in Ref. [13] and summarized here. Generic correlation functions can be viewed as products of creation and annihilation operators with many transfer matrix factors describing Euclidean time evolution. It is difficult to understand the distribution of products of transfer matrices in quantum field theories, but heuristically one can naively picture a late-time correlation function as a product of random numbers representing the action of the transfer matrix on the ground state (dominating the late-time behavior of the correlation function). As a further simplification, one can consider products of transfer matrices describing time evolution over a period larger than the dynamical correlation length of the theory in question, and heuristically view a correlation function as a product of independent, identically distributed random numbers that each represent time evolution of the ground

state over a period longer than a correlation length. Application of the central limit theorem to the logarithm of a product of many independent, identically distributed random numbers shows that the logarithm of the product tends to become normally distributed as the number of factors becomes large. Therefore, naively, the correlation function itself should tend to become log-normal as the number of transfer matrix factors becomes large [13]. This argument in particular assumes that the random variables in question originate from distributions that have a finite variance so that the central limit theorem applies. A generalized central limit theorem proves that sums of heavy-tailed random variables tend to become distributed according to stable distributions (that include the normal distribution as a special case).

Stable distributions are named as such because their shape is stable under averaging of independent copies of a random variable. Formally, stable distributions form a manifold of fixed points in a Wilsonian space of probability distributions where averaging independent random variables from the distribution plays the role of renormalization group evolution. A parameter α , called the index of stability, dictates the shape of a stable distribution and remains fixed under averaging transformations. All probability distributions with finite variance evolve under averaging towards the normal distribution, a special case of the stable distribution with $\alpha = 2$. Heavy-tailed distributions with ill-defined variance evolve towards generic stable distributions with $0 < \alpha \leq 2$. In particular, stable distributions with $\alpha < 2$ have power-law tails; for a stable random variable X the tails decay as $X^{-(\alpha+1)}$. The heavy-tailed Cauchy, Levy, and Holtsmark distributions are special cases of stable distributions with $\alpha = 1$, $1/2$, and $3/2$ respectively, that arise in physical applications.⁵

Stable distributions for a real random variable X are defined via Fourier transform,

$$\mathcal{P}_S(X; \alpha, \beta, \mu, \gamma) = \int \frac{dk}{2\pi} e^{-ikX} \Phi_X(k; \alpha, \beta, \mu, \gamma) \quad , \quad (20)$$

of their characteristic functions

$$\Phi_X(k; \alpha, \beta, \mu, \gamma) = \exp \left(i\mu k - |\gamma k|^\alpha \left[1 - i\beta \frac{k}{|k|} \tan(\pi\alpha/2) \right] \right) \quad , \quad (21)$$

where $0 < \alpha \leq 2$ is the index of stability, $-1 \leq \beta \leq 1$ determines the skewness of the distribution, μ is the location of peak probability, γ sets the width. For $\alpha = 1$, the above parametrization does not hold and $\tan(\pi\alpha/2)$ should be replaced by $-\frac{2}{\pi} \ln |k|$. For $\alpha > 1$ the mean is μ , and for $\alpha \leq 1$ the mean is ill-defined. For $\alpha = 2$ the variance is $\sigma^2 = \gamma^2/2$ and Eq. (21) implies the distribution is independent of β , while for $\alpha < 2$ the variance is ill-defined.

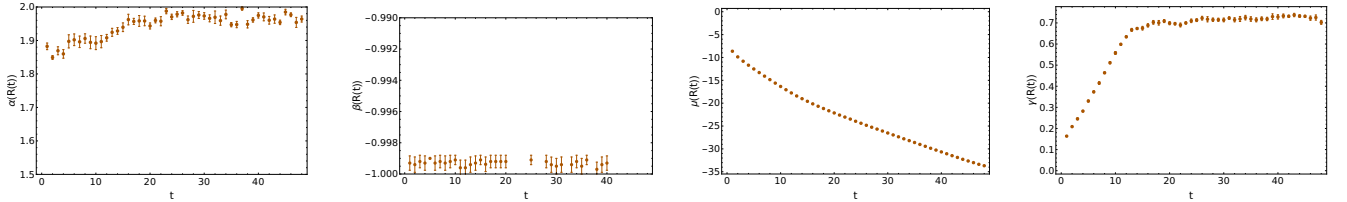


FIG. 14: Maximum likelihood estimates for stable distribution fits of $R(t)$ in terms of the parameters of Eq. (20)-(21). $\alpha = 2$ corresponds to a normal distribution. The associated uncertainties are estimated by bootstrap methods. Changes in β do not affect the likelihood when $\alpha = 2$, and reliable estimates of $\beta(R(t))$ are not obtained at all times.

The distributions of $R(t)$ obtained from the LQCD calculations can be fit to stable distributions through maximum likelihood estimation of the stable parameters α , β , μ , and γ , obtaining the results that are shown in Fig. 14. Estimates of $\alpha(R(t))$ are consistent with 2, corresponding to a normal distribution. This is not surprising, because higher moments of $|C(t)|$ would be ill-defined and diverge in the infinite statistics limit if $R(t)$ were literally described by a heavy-tailed distribution. $\beta(R(t))$ is strictly ill-defined when $\alpha(R(t)) = 2$, but results consistent with $\beta(R(t)) = -1$ indicate negative skewness in agreement with observations above. Estimates of $\mu(R(t))$ and $\gamma(R(t))$ are consistent with the cumulant results above if a normal distribution ($\alpha(R(t)) = 2$) is assumed. Fits of $R(t)$ to generic stable distributions are shown in Fig. 9, and are roughly consistent with fits to a normal distribution, though some skewness is captured by the stable fits.

⁵ Further details can be found in textbooks and reviews on stable distributions and their applications in physics. See, for instance, Refs. [38–42] and references within.

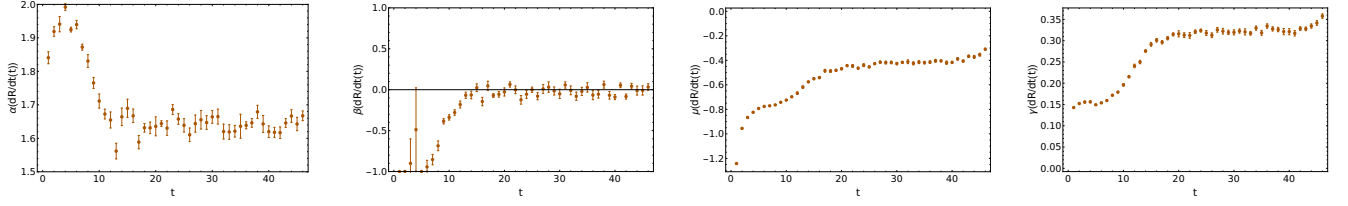


FIG. 15: Maximum likelihood estimates for stable distribution fits of $\frac{dR}{dt}$ similar to Fig. 14. The associated uncertainties are estimated by bootstrap methods.

Stable distribution fits to $\frac{dR}{dt}$ indicate statistically significant deviations from a normal distribution ($\alpha = 2$), as seen in Fig. 15. The late-time distribution of $\frac{dR}{dt}$ appears time independent, and fitting $\alpha(\frac{dR}{dt})$ in the late-time plateau region gives an estimate of the late-time index of stability. Recalling $\frac{dR}{dt}$ describes a finite difference over a physical time interval of one lattice spacing, the estimated index of stability is

$$\alpha(\Delta R(t \rightarrow \infty, \Delta t \sim 0.12 \text{ fm})) \rightarrow 1.639(4)(1). \quad (22)$$

Maximum likelihood estimates for $\mu(\frac{dR}{dt})$ are consistent with the sample mean, and $\beta(\frac{dR}{dt})$ is consistent with zero in agreement with observations of vanishing skewness. Therefore, the distribution of $\frac{dR}{dt}$ is symmetric, as observed in Fig. 13, with power-law tails scaling as $\sim (\Delta R)^{-2.65}$ over this time interval of $\Delta t \sim 0.12 \text{ fm}$.

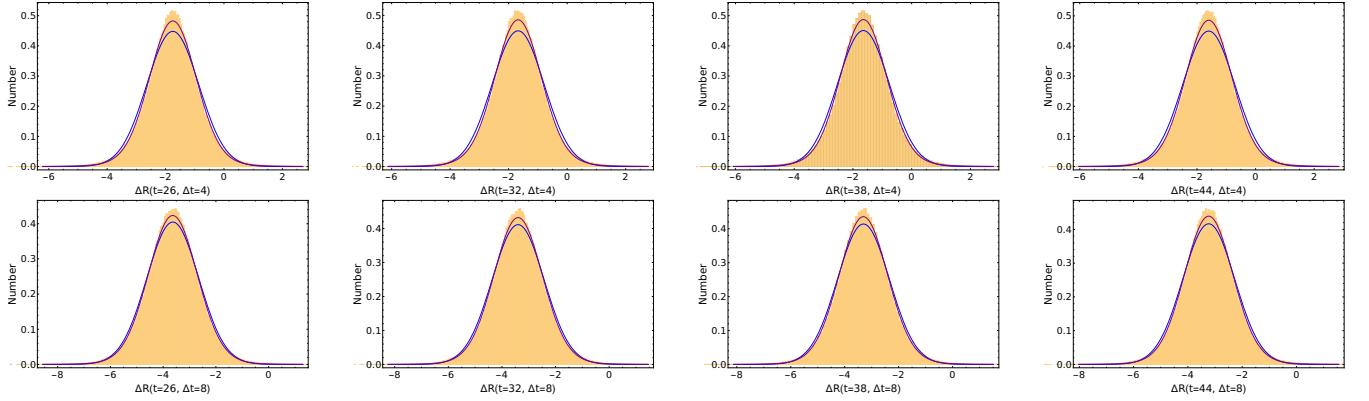


FIG. 16: Histograms of $\Delta R(t, \Delta t)$ for selected late-time values of t . The top row shows results for $\Delta t = 4$, the bottom row shows results for $\Delta t = 8$, and Fig. 13 shows the results for $\Delta t = 1$. The blue curves represent fits to a normal distribution, while the purple curves represent fits to a stable distribution.

The value of $\alpha(\frac{dR}{dt})$ depends on the physical time separation used in the finite difference definition Eq. (18), and stable distribution fits can be performed for generic finite differences $\Delta R(t, \Delta t)$. For all Δt , the distribution of ΔR becomes time independent at late times. Histograms of the late-time distributions ΔR for $\Delta t = 4, 8$ are shown in Fig. 16, and the best fit late-time values for $\alpha(\Delta R)$ and $\gamma(\Delta R)$ are shown in Fig. 17. Since QCD has a finite correlation length, $\Delta R(t, \Delta t)$ can be described as the difference of approximately normally distributed variables at large Δt . In the large Δt limit, ΔR is therefore necessarily almost normally distributed, and correspondingly, $\alpha(\Delta R)$, shown in Fig. 17, increases with Δt and appears to approach the normal distribution value $\alpha(\Delta R) \rightarrow 2$ for large Δt . Heavy-tailed distributions are found to be needed only to describe the distribution of ΔR when Δt is small enough such that $R(t)$ and $R(t - \Delta t)$ are physically correlated. In some sense, the deviations from normally distributed differences, i.e. $\alpha(\Delta R) < 2$, are a measure the strength of dynamical QCD correlations on the scale Δt .

The heavy-tailed distributions of ΔR for dynamically correlated time separations correspond to time evolution $\frac{dR}{dt}$ that is quite different to that of diffusive Brownian motion describing the quantum mechanical motion of free point particles. Rather than Brownian motion, heavy-tailed jumps in $R(t)$ correspond to a superdiffusive random walk or Lévy flight. Power-law, rather than exponentially suppressed, large jumps give Lévy flights a qualitatively different character than diffusive random walks, including fractal self-similarity, as can be seen in Fig. 18. The dynamical features of QCD that give rise to superdiffusive time evolution are presently unknown, however, we conjecture that instantons play a role, and it would be interesting to understand if $\alpha(\frac{dR}{dt})$ can be simply related to observable properties

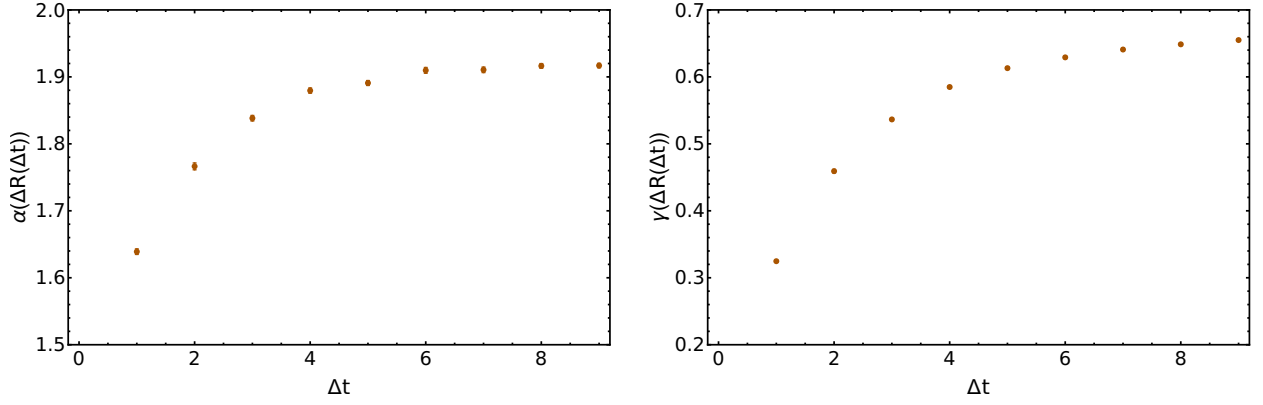


FIG. 17: Maximum likelihood estimates for the index of stability, $\alpha(\Delta R(t, \Delta t))$ and width $\gamma(\Delta R(t, \Delta t))$, in the late-time plateau region as a function of Δt . Associated uncertainties are estimated with bootstrap methods.

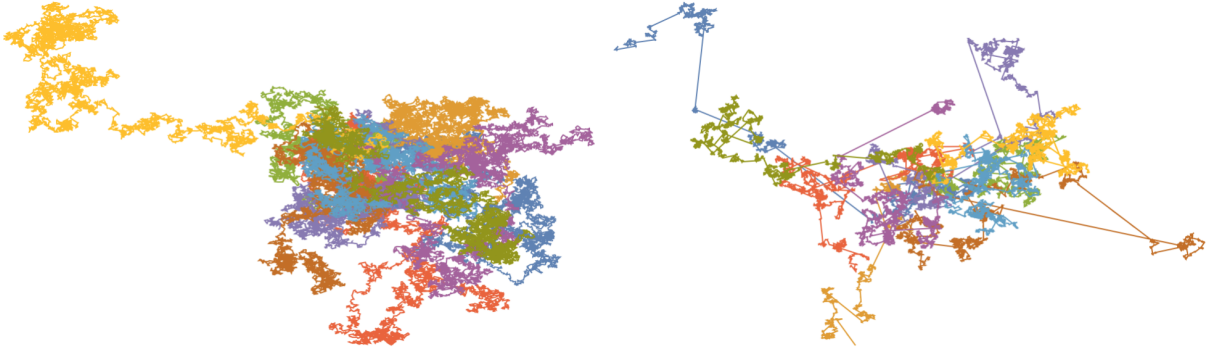


FIG. 18: The two-dimensional motion of tests particles with their random motion taken from symmetric Stable Distributions. At each time step, the angle of the outgoing velocity is chosen randomly with respect to the incident velocity while the magnitude of the velocity is chosen from a symmetric Stable Distribution with $\alpha = 2$ corresponding to Brownian motion (left panel), and $\alpha = 1.5$ corresponding to a Holtsmark distribution (right panel). In the right panel, the large separations between clusters achieved during one time interval correspond to Lévy flights.

of the nucleon. It is also not possible to say from this single study whether $\alpha(\frac{dR}{dt})$ has a well-defined continuum limit for infinitesimal Δt . Further LQCD studies are required to investigate the continuum limit of $\alpha(\frac{dR}{dt})$. Lattice field theory studies of other systems and calculations of $\alpha(\frac{dR}{dt})$ in perturbation theory, effective field theory, and models of QCD could provide important insights into the dynamical origin of superdiffusive time evolution.⁶

One feature of LQCD $\frac{dR}{dt}$ results is not well described by a stable distribution. The variance of heavy-tailed distributions is ill-defined, and were $\frac{dR}{dt}$ truly described by a heavy-tailed distribution then the variance and higher cumulants of $\frac{dR}{dt}$ would increase without bound as the size of the statistical ensemble is increased. This behavior is not observed. While the distribution of $\frac{dR}{dt}$ is well-described by a stable distribution near its peak, the extreme tails of the distribution of $\frac{dR}{dt}$ decay sufficiently quickly that the variance and higher cumulants of $\frac{dR}{dt}$ shown in Fig. 12 give statistically consistent results as the statistical ensemble size is varied. This suggests that $\frac{dR}{dt}$ is better described by a truncated stable distribution, a popular model for, for example, financial markets exhibiting high volatility but with a natural cutoff on trading prices, in which some form of sharp cutoff is added to the tails of a stable distribution [41]. Note that the tails of the $\frac{dR}{dt}$ distribution describe extremely rapid changes in the correlation function and are sensitive to ultraviolet properties of the theory. It is plausible that a truncated stable distribution arises because the lattice

⁶ For example, an analysis of pion correlation functions from the same ensemble of gauge-field configurations shows that R and $\frac{dR}{dt}$ are both approximately normally distributed, with $\alpha = 1.96(1)$ and $\alpha = 1.97(1)$, respectively. We conclude that the pion shows only small deviations from free particle Brownian motion.

regulator adds a sharp cutoff to the power-law decay of the distribution at very large $\frac{dR}{dt}$. Further studies at different lattice spacings will be needed to understand the form of the truncation and whether the truncation scale is indeed set by the lattice scale. It is also plausible that there is a strong interaction length scale providing a modification to the distribution at large $\frac{dR}{dt}$. For now we simply observe that a truncated stable distribution with an unspecified high-scale modification provides a very good empirical description of $\frac{dR}{dt}$.

Before turning to the complex phase of $C(t)$, we summarize the main findings about the log-magnitude:

- The log-magnitude of the nucleon correlation function in LQCD is approximately normally distributed with small but statistically significant negative skewness and positive kurtosis.
- The magnitude effective mass $m_R(t)$ approaches $\frac{3}{2}m_\pi$ at late times, consistent with expectations from Parisi-Lepage scaling for the nucleon variance $|C(t)|^2 \sim e^{-3m_\pi t}$. The plateau of $m(t)$ marks the start of the golden window where excited state systematics are negligible and statistical uncertainties are increasing slowly. The much later plateau of $m_R(t)$ roughly coincides with the plateau of $m_\theta(t)$ to $m_N - \frac{3}{2}m_\pi$ and occurs after variance growth of $m(t)$ reaches the Parisi-Lepage expectation $e^{2(m_N - \frac{3}{2}m_\pi)t}$. Soon after, a noise region begins where the variance of $m(t)$ stops increasing and the effective mass cannot be reliably estimated.
- The log-magnitude does not have a severe StN problem, and $m_R(t)$ can be measured accurately across all 48 timesteps of the present LQCD calculations. The variance of the log-magnitude distribution only increases by a few percent in 20 timesteps after visibly plateauing.
- The cumulant expansion describes $m(t)$ as a sum of the time derivatives of the cumulants of the log of the correlation function. At late times, the time derivative of the mean of $R(t)$ is constant and approximately equal to $m_R(t)$. Contributions to $m_R(t)$ from the variance and higher cumulants of $R(t)$ are barely resolved in the sample of 500,000 correlation functions.
- Finite differences in $R(t)$, $\Delta R(t, \Delta t)$, are described by time independent distributions at late times. For large Δt compared to the QCD correlation length, ΔR describes a difference of approximately independent normal random variables and is therefore approximately normally distributed. For small Δt , ΔR describes a difference of dynamically correlated variables. The mean of $\frac{dR}{dt}$ is equal to the time derivative of the mean of $R(t)$ and therefore provides a good approximation to $m_R(t)$. The time derivatives of higher cumulants of $R(t)$ cannot be readily extracted from cumulants of $\frac{dR}{dt}$ without knowledge of dynamical correlations.
- At late times, $\frac{dR}{dt}$ is well described by a symmetric, heavy-tailed, truncated stable distribution. The presence of heavy tails in $\frac{dR}{dt}$ indicates that $R(t)$ is not described by free particle Brownian motion but rather by a superdiffusive Lévy flight. Deviations of the index of stability of $\frac{dR}{dt}$ from a normal distribution quantify the amount of dynamical correlations present in the nucleon system, the physics of which is yet to be understood. Further studies are required to determine the continuum limit value of the index of stability associated with $\frac{dR}{dt}$ and the dynamical origin and generality of superdiffusive Lévy flights in quantum field theory correlation functions.

B. The Phase

The reality of average correlation functions requires that the distribution of $\theta(t)$ be symmetric under $\theta(t) \rightarrow -\theta(t)$. Cumulants of $\theta(t)$ calculated from sample moments in analogy to Eq. (14) are shown in Fig. 19. The mean and κ_3

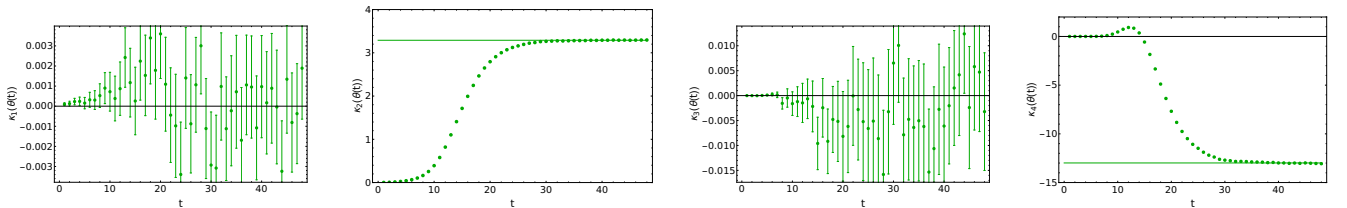


FIG. 19: The first four cumulants of $\theta(t)$. In these fits, no special care is given to the fact that $\theta(t)$ is a phase defined on $-\pi < \theta(t) \leq \pi$ and standard sample moments are used to determine these cumulants in analogy to Eq. (14). Uniform distribution results of $\frac{\pi^2}{3}$ variance and $-\frac{2\pi^4}{15}$ fourth cumulant are shown as green lines for reference.

are noisy but statistically consistent with zero as expected. The variance and κ_4 are small at early times since every sample of $\theta(t)$ is defined to vanish at $t = 0$, and grow linearly at intermediate times $10 < t < 20$ around the golden window. After $t = 20$, this linear growth slows and they become constant at late times, and are consistent with results from a uniform distribution. Histograms of $\theta(t)$ shown in Fig. 20 qualitatively suggest that $\theta(t)$ is described

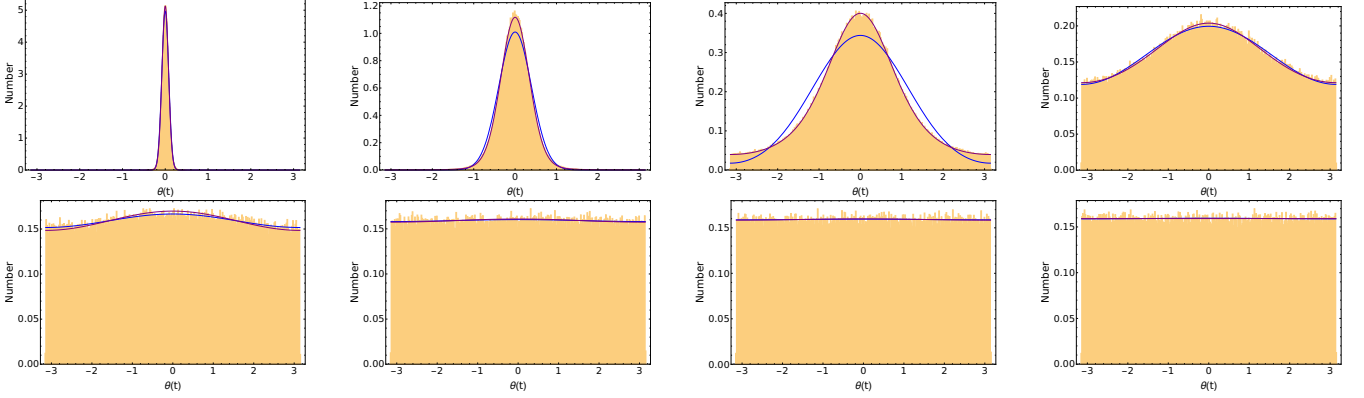


FIG. 20: Histograms of $\theta(t)$ with fits to wrapped normal distributions using Eq. (27) shown in blue and fits to wrapped stable distributions using maximum likelihood estimation of the parameters of Eq. (37) shown in purple. See the main text for details.

by a narrow, approximately normal distribution at early times and an increasingly broad, approximately uniform distribution at late times. $\theta(t)$ is only defined modulo 2π and can be described as a circular variable defined on the interval $-\pi < \theta \leq \pi$. The distribution of $\theta(t)$ can therefore be described with angular histograms, as shown in Fig. 21. Again, $\theta(t)$ resembles a uniform circular random variable at late times.

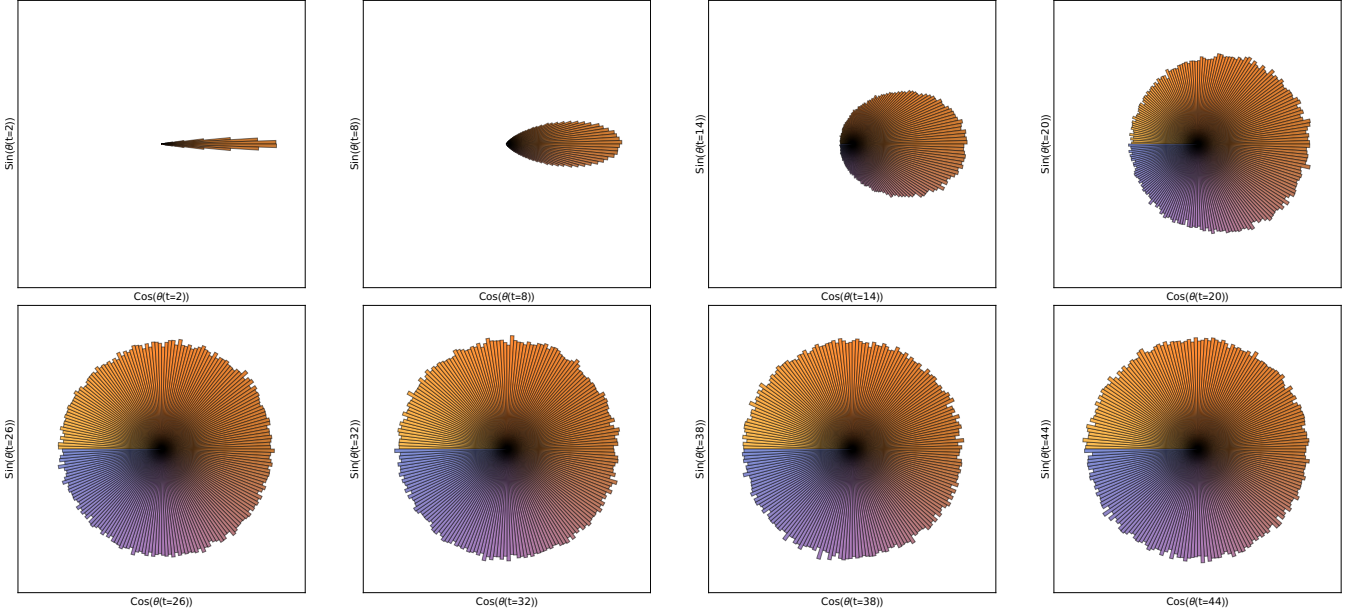


FIG. 21: Angular histograms of $\theta(t)$. The unit circle $[0, 2\pi)$ is split into a uniform sequence of bins, and the number of $\theta(t)$ samples falling in each bin sets the radial length of a bar at that angle.

A cumulant expansion can be readily constructed for $m_\theta(t)$. The mean phase is given in terms of the characteristic function and cumulants of $\theta(t)$ by

$$\langle e^{i\theta(t)} \rangle = \Phi_{\theta(t)}(1) = \exp \left[\sum_{n=0}^{\infty} \frac{i^n}{n!} \kappa_n(\theta(t)) \right] , \quad (23)$$

and the appropriate cumulant expansion for $m_\theta(t)$ is therefore, using Eq. (12),

$$m_\theta(t) = \sum_{n=0}^{\infty} \frac{i^n}{n!} [\kappa_n(\theta(t)) - \kappa_n(\theta(t+1))] \quad . \quad (24)$$

Factors of i^n dictate that a linearly increasing variance of $\theta(t)$ makes a positive contribution to $m_\theta(t)$, in contradistinction to the slight negative contribution to $m_R(t)$ made by linearly increasing variance of $R(t)$. Since the mean of $\theta(t)$ necessarily vanishes, the variance of $\theta(t)$ makes the dominant contribution to Eq. (24) for approximately normally distributed $\theta(t)$. For this contribution to be positive, the variance of $\theta(t)$ must increase, indicating that $\theta(t)$ has a StN problem. For the case of approximately normally distributed $\theta(t)$, non-zero m_θ requires a StN problem for the phase.

Contributions to Eq. (24) from the first four cumulants of $\theta(t)$ are shown in Fig. 22. Contributions from odd cumulants are consistent with zero, as expected by $\theta(t) \rightarrow -\theta(t)$ symmetry. The variance provides the dominant contribution to $m_\theta(t)$ at early and intermediate times, and is indistinguishable from the total $m_\theta(t)$ calculated using the standard effective mass estimator for $t \lesssim 15$. Towards to end of the golden window $15 \lesssim t \lesssim 25$, the variance contribution to the effective mass begins to decrease. At very late times $t \gtrsim 30$ contributions to $m_\theta(t)$ from the variance are consistent with zero. The fourth cumulant makes smaller but statistically significant contributions to $m_\theta(t)$ at intermediate times. Contributions from the fourth cumulant also decrease and are consistent with zero at late times. The vanishing of these contributions results from the distribution becoming uniform at late times, and time independent as a consequence. These observations signal a breakdown in the cumulant expansion at late times $t \gtrsim 25$ where contributions from the variance do not approximate standard estimates of $m_\theta(t)$. Notably, the breakdown of the cumulant expansion at $t \gtrsim 25$ coincides with plateaus to uniform distribution cumulants in Fig. 19 and with the onset of the noise region discussed in Sec. III.

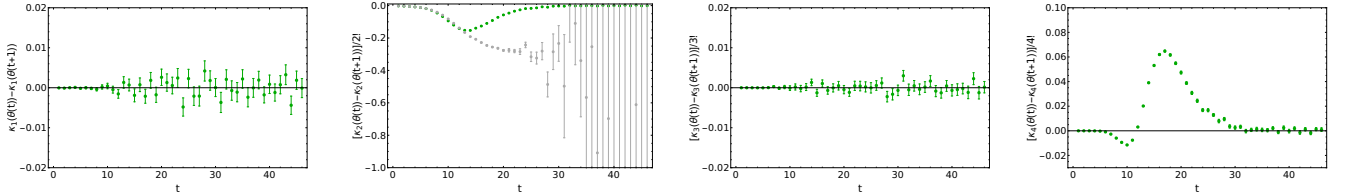


FIG. 22: Contributions from the first four terms in the cumulant expansion of Eq. (17). The variance, shown second from left, is expected to provide the dominant contribution if a truncation of Eq. (17) is reliable. Standard estimates of $m_\theta(t)$ from Eq. (12) are shown as the gray points, alongside the cumulant contribution (green points) in the second from left panel. Other panels only show cumulant contributions (green points).

Observations of these unexpected behaviors of $\theta(t)$ in the noise region hint at more fundamental issues with the statistical description of $\theta(t)$ used above. A sufficiently localized probability distribution of a circular random variable peaked far from the boundaries of $-\pi < \theta(t) \leq \pi$ can be reliably approximated as a standard probability distribution of a linear random variable defined on the real line. For broad distributions of a circular variable, the effects of a finite domain with periodic boundary conditions cannot be ignored. While circular random variables are not commonly encountered in quantum field theory, they arise in many scientific contexts, most notably in astronomy, biology, geography, geology, meteorology and oceanography. Familiarity with circular statistics is not assumed here, and a few basic results relevant for understanding the statistical properties of $\theta(t)$ will be reviewed without proof. Further details can be found in Refs. [21–23] and references therein.

A generic circular random variable θ can be described by two linear random variables $\cos(\theta)$ and $\sin(\theta)$ with support on the line interval $[-1, 1]$ where periodic boundary conditions are not imposed. It is the periodic identification of $\theta = \pm\pi$ that makes sample moments poor estimators of the distribution of θ and, in particular, allows the sample mean of a distribution symmetrically peaked about $\theta = \pm\pi$ to be opposite the actual location of peak probability. Parameter estimation for circular distributions can be straightforwardly performed using trigonometric moments of $\cos(\theta)$ and $\sin(\theta)$. For an ensemble of N random angles θ_i , the first trigonometric moments are defined by the sample averages,

$$\bar{C} = \frac{1}{N} \sum_i \cos(\theta_i), \quad \bar{S} = \frac{1}{N} \sum_i \sin(\theta_i) \quad . \quad (25)$$

Higher trigonometric moments can be defined analogously but will not be needed here. The average angle can be defined in terms of the mean two-dimensional vector (\bar{C}, \bar{S}) as

$$\bar{\theta} = \arg(\bar{C} + i\bar{S}) \quad . \quad (26)$$

A standard measure of a circular distribution's width is given in terms of trigonometric moments as

$$\bar{\rho}^2 = \bar{\mathcal{C}}^2 + \bar{\mathcal{S}}^2 \quad (27)$$

where $\bar{\rho}$ should be viewed as a measure of the concentration of a circular distribution. Smaller $\bar{\rho}$ corresponds to a broader, more uniform distribution, while larger $\bar{\rho}$ corresponds to a more localized distribution.

One way of defining statistical distributions of circular random variables is by “wrapping” distributions for linear random variables around the unit circle. The probability of a circular random variable equaling some value in $-\pi < \theta \leq \pi$ is equal to the sum of the probabilities of the linear random variable equaling any value that is equivalent to θ modulo 2π . Applying this prescription to a normally distributed linear random variable gives the wrapped normal distribution

$$\mathcal{P}_{WN}(\theta; \mu, \sigma) = \frac{1}{\sqrt{2\pi}\sigma} \sum_{k=-\infty}^{\infty} \exp \left[-\frac{(\theta - \mu + 2\pi k)^2}{2\sigma^2} \right] = \frac{1}{2\pi} \sum_{n=-\infty}^{\infty} e^{in(\theta - \mu) - \sigma^2 n^2 / 2} \quad , \quad (28)$$

where the second form follows from the Poisson summation formula. Wrapped distributions share the same characteristic functions as their unwrapped counterparts, and the second expression above can be derived as a discrete Fourier transform of a normal characteristic function. The second sum above can also be compactly represented in terms of elliptic- ϑ functions. For $\sigma^2 \lesssim 1$ the wrapped normal distribution qualitatively resembles a normal distribution, but for $\sigma^2 \gtrsim 1$ the effects of wrapping obscure the localized peak. As $\sigma^2 \rightarrow \infty$, the wrapped normal distribution becomes a uniform distribution on $(-\pi, \pi]$. Arbitrary trigonometric moments and therefore the characteristic function of the wrapped normal distribution are given by

$$\langle e^{in\theta} \rangle_{WN} = e^{in\mu - n^2 \sigma^2 / 2} \quad . \quad (29)$$

Parameter estimation in fitting a wrapped normal distribution to LQCD results for $\theta(t)$ can be readily performed by relating $\bar{\theta}$ and $\bar{\rho}$ above to these trigonometric moments as

$$\mu = \bar{\theta} \quad \text{and} \quad e^{-\sigma^2} = \bar{\rho}^2 \quad . \quad (30)$$

Note that Eq. (30) holds only in the limit of infinite statistics. Estimates for the average of a wrapped normal distribution are consistent with zero at all times, as expected. Wrapped normal probability distribution functions with $\sigma^2(\theta(t))$ determined from Eq. (30) are shown with the histograms of Fig. 20 and provide a good fit to the data at all times.

The appearance of a uniform distribution at late times is consistent with the heuristic argument that the logarithm of a correlation function should be described by a stable distribution. The uniform distribution is a stable distribution for circular random variables, and in fact is the only stable circular distribution [23]. The distribution describing a sum of many linear random variables broadens as the number of summands is increased, and the same is true of circular random variables. A theorem of Poincaré proves that as the width of any circular distribution is increased without bound, the distribution will approach a uniform distribution. One therefore expects that the sum of many well-localized circular random variables might initially tend towards a narrow wrapped normal distribution while boundary effects are negligible. Eventually as more terms are added to the sum this wrapped normal distribution will broaden and approach a uniform distribution. This intuitive picture appears consistent with the time evolution of $\theta(t)$ shown in Figs. 20, 21.

The wrapped normal variance estimates for $\theta(t)$ that are shown in Fig. 23 require further discussion. At intermediate times, the wrapped normal variance calculated from Eq. (30) rises linearly with a slope consistent with $m_N - \frac{3}{2}m_\pi$. This is not surprising because assuming an exactly wrapped normal $\theta(t)$, $m_\theta(t)$ becomes

$$m_\theta^{WN}(t) = \ln \left[\frac{\langle e^{i\theta(t)} \rangle_{WN}}{\langle e^{i\theta(t+1)} \rangle_{WN}} \right] = -\frac{1}{2} [\sigma^2(\theta(t)) - \sigma^2(\theta(t+1))] \quad . \quad (31)$$

Eq. (31) resembles the first non-zero term in the cumulant expansion given in Eq. (24) adapted for circular random variables. Results for $m_\theta^{WN}(t)$ are also shown in Fig. 23, where it is seen that $m_\theta^{WN}(t)$ is indistinguishable from $m_\theta(t)$ at early and intermediate times. In the noise region, both $m_\theta^{WN}(t)$ and standard estimates for $m_\theta(t)$ are consistent with zero. $m_\theta(t)$ has smaller variance than $m_\theta^{WN}(t)$ in the noise region, but this late time noise is the only visible signal of deviation between the two. This is not surprising, because $m_\theta^{WN}(t)$ is actually identical to $m_\theta(t)$ when $\bar{\mathcal{S}}(\theta(t)) = 0$. Since $\bar{\mathcal{S}}(\theta(t))$ vanishes in the infinite statistics limit by $\theta(t) \rightarrow -\theta(t)$ symmetry, $m_\theta^{WN}(t)$ must agree with $m_\theta(t)$ up to statistical noise. At late times $t \gtrsim 30$, the wrapped normal variance shown in Fig. 23 becomes roughly constant up to sizable fluctuations. The region where $\sigma^2(\theta(t))$ stops increasing coincides with the noise region previously identified.

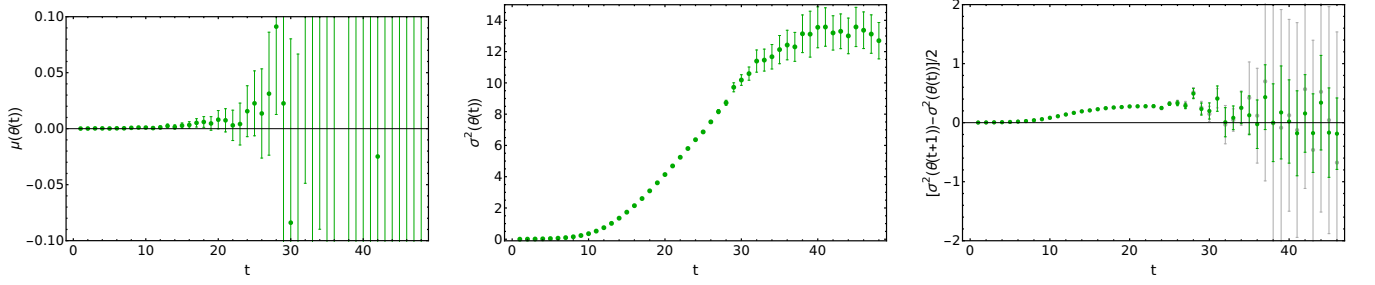


FIG. 23: The left panel shows estimates of the wrapped normal mean $\mu(\theta(t))$ calculated from Eq. (30) as a function of time. The center panel shows analogous estimates of the wrapped normal variance, $\sigma^2(\theta(t))$. The right panel shows the wrapped normal effective mass, $m_\theta^{WN}(t)$, defined in Eq. (31) (green points) along with the standard complex phase effective mass $m_\theta(t)$ defined in Eq. (24) (gray points).

The time at which the noise region begins depends on the size of the statistical ensemble N . Figure 24 shows estimates of $\sigma^2(\theta(t))$ from Eq. (30) for statistical ensemble sizes $N = 50, 5,000, 500,000$ varying across four orders of magnitude. The time of the onset of the noise region varies logarithmically as $t \sim 20, 27, 35$. The constant noise region value of $\sigma^2(\theta(t))$ is also seen to vary logarithmically with N . Equality of $m_\theta^{WN}(t)$ and $m_\theta(t)$ up to statistical fluctuations shows that $m_\theta(t)$ must be consistent with zero in the noise region. Since corrections to $m(t) \approx m_\theta(t) + m_R(t)$ from magnitude-phase correlations appear small at all times, it is reasonable to conclude that standard estimators for the nucleon effective mass are systematically biased in the noise region and that exponentially large increases in statistics are required to delay the onset of the noise region.

Besides these empirical observations, the inevitable existence and exponential cost of delaying the noise region can be understood from general arguments of circular statistics. The expected value of the sample concentration $\bar{\rho}^2$ can be calculated by applying Eq. (29) to an ensemble of independent wrapped normal random variables θ_i in Eq. (27). The result shows that $\bar{\rho}^2$ is a biased estimate of $e^{-\sigma^2}$, and that the appropriate unbiased estimator is [21, 23]

$$e^{-\sigma^2} = \frac{N}{N-1} \left(\bar{\rho}^2 - \frac{1}{N} \right). \quad (32)$$

For $\bar{\rho}^2 < 1/N$, Eq. (32) would lead to an imaginary estimate for σ^2 and therefore no reliable unbiased estimate can be extracted. A similar calculation shows that the expected variance of $\bar{\rho}^2$ is

$$\text{Var}(\bar{\rho}^2) = \frac{N-1}{N^3} (1 - e^{-\sigma^2})^2 \left[(1 - e^{-\sigma^2})^2 + 2Ne^{-\sigma^2} \right]. \quad (33)$$

In the limit of an infinitely broad distribution, all circular distributions tend towards uniform and the variance of $\bar{\rho}^2$ is set by the $\sigma^2 \rightarrow \infty$ limit of Eq. (33) regardless of the form of the true underlying distribution. When analyzing any very broad circular distribution, measurements of $\bar{\rho}^2$ will therefore include fluctuations on the order of $1/N$. For $e^{-\sigma^2} < 1/N$, the expected error from finite sample size effects in statistical inference based on $\bar{\rho}^2$ is therefore larger than the signal to be measured. In this regime $\bar{\rho}^2$ has both systematic bias and expected statistical errors that are larger than the value $e^{-\sigma^2}$ that $\bar{\rho}^2$ is supposed to estimate. $\bar{\rho}^2$ cannot provide accurate estimates of $e^{-\sigma^2}$ in this regime.

Inability to perform statistical inference in the regime $e^{-\sigma^2} < 1/N$ matters for the nucleon correlation function because $e^{-\sigma^2(\theta(t))} = \bar{\rho}^2(\theta(t)) = \langle \cos(\theta(t)) \rangle^2$ and therefore $e^{-\sigma^2(\theta(t))}$ decreases exponentially with time. At late times there will necessarily be a noise region where $e^{-\sigma^2(\theta(t))} < 1/N$ is reached and $\bar{\rho}^2(\theta(t))$ is not a reliable estimator. Keeping $e^{-\sigma^2(\theta(t))}$ larger than the bias and expected fluctuations of $\bar{\rho}^2(\theta(t))$ requires

$$N > e^{\sigma^2(\theta(t))} \sim e^{2(m_N - \frac{3}{2}m_\pi)t}. \quad (34)$$

Eq. (34) demonstrates that exponential increases in statistics are required to delay the time where statistical uncertainties and systematic bias dominate physical results estimated from $\bar{\rho}^2(\theta(t))$. Formally, the noise region can be defined as the region where Eq. (34) is violated. Lines at $\sigma^2(\theta(t)) = \ln N$ are shown on Fig. 24 for the ensembles with $N = 50, 5,000, 500,000$ shown. By this definition, the noise region formally begins once $\sigma^2(\theta(t))$ (extrapolated from reliable estimates in the golden window) crosses above the appropriate line. Excellent agreement can be seen between this definition and the above empirical characterizations of the noise region based on constant $\sigma^2(\theta(t))$ and unreliable effective mass estimates with constant errors.

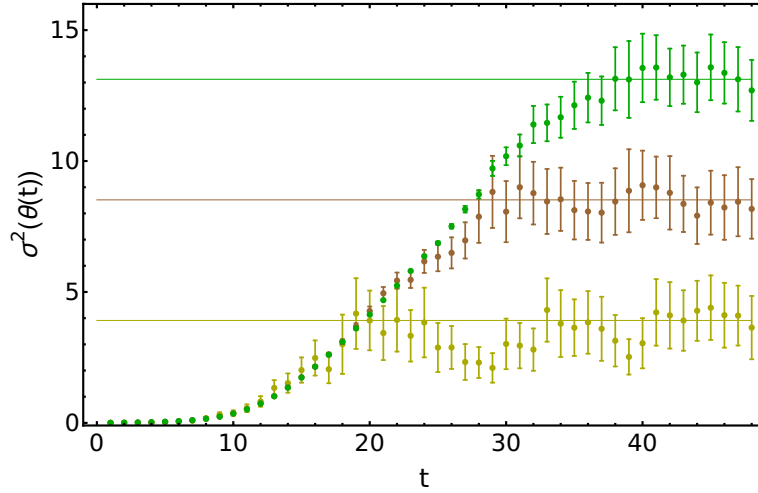


FIG. 24: Wrapped normal variance of the phase $\sigma^2(\theta(t))$ for statistical ensembles of various sizes. Results for an ensemble of $N = 50$ nucleon correlation functions are shown in yellow, $N = 5,000$ in brown, and $N = 500,000$ in green. Lines of each color are also shown at $\sigma^2(\theta(t)) = \ln(N)$. Above the relevant line, Eq. (34) is violated for each ensemble and measurements of $\sigma^2(\theta(t))$ are expected to be roughly equal to $\ln(N)$ instead of the underlying physical value of $\sigma^2(\theta(t))$. Estimates of $\sigma^2(\theta(t))$ reaching these lines marks the beginning of the noise region defined by violations of Eq. (34) for each ensemble.

Breakdown of statistical inference for sufficiently broad distributions is a general feature of circular distributions. Fisher notes that circular distributions are distinct from more familiar linear distributions in that “formal statistical analysis cannot proceed” for sufficiently broad distributions [21]. The arguments above do not rely on the particular form of the wrapped normal model assumed for $\theta(t)$, and the basic cause for the onset of the noise region for broad $\theta(t)$ is that $\bar{\rho}^2$ has an uncertainty of order $1/N$ for any broad circular distribution that begins approaching a uniform distribution.⁷ Analogs of Eq. (34) can be expected to apply to statistical estimation of the mean of any complex correlation function. As long as the asymptotic value of m_θ is known, Eq. (34) and analogs for other complex correlation functions can be used to estimate the required statistical ensemble size necessary to reliably estimate the mean correlation function up to a desired time t .

The pathological features of the late-time distribution of $\theta(t)$ are not shared by $\frac{d\theta}{dt}$. As with the log-magnitude, it is useful to define general finite differences,

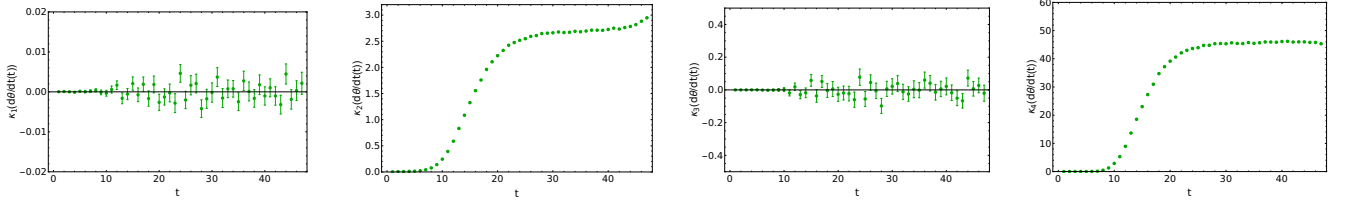
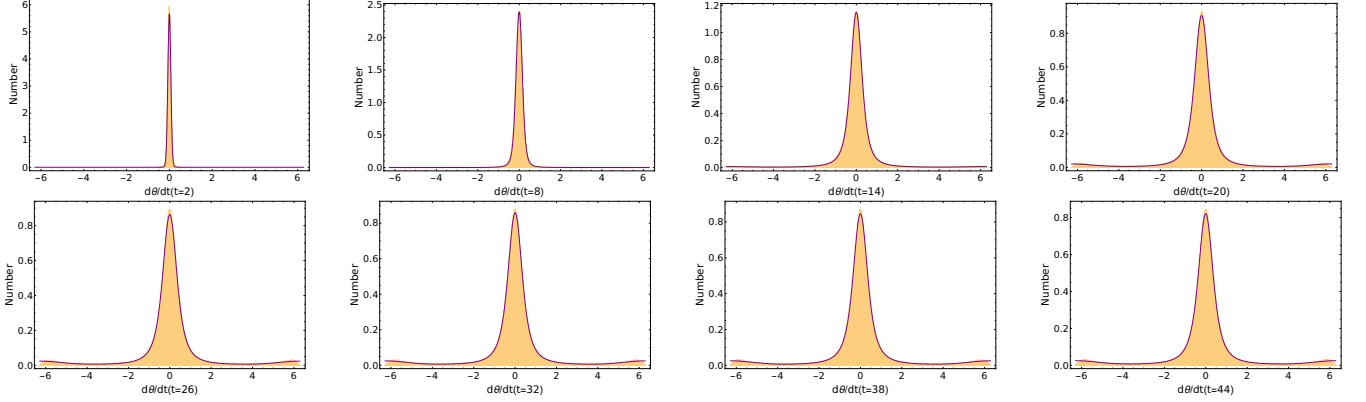
$$\Delta\theta(t, \Delta t) = \theta(t) - \theta(t - \Delta t) \quad , \quad (35)$$

and a discrete (lattice) time derivative,

$$\frac{d\theta}{dt} = \Delta\theta(t, 1) \quad . \quad (36)$$

The sample cumulants of $\frac{d\theta}{dt}$ are shown in Fig. 25, histograms of $\frac{d\theta}{dt}$ are shown in Fig. 26, and angular histograms are shown in Fig. 27. Much like $\frac{dR}{dt}$, $\frac{d\theta}{dt}$ appears to have a time independent distribution at late times. While $\frac{d\theta}{dt}$ is a circular random variable, its distribution is still well-localized at late times and can be clearly visually distinguished from a uniform distribution. This suggests that statistical inference of $\frac{d\theta}{dt}$ should be reliable in the noise region.

⁷ One may wonder whether there is a more optimal estimator than $\bar{\rho}^2$ that could reliably calculate the width of broad circular distributions with smaller variance. While this possibility cannot be discarded in general, it is interesting to note that it can be in one model. The most studied distribution in one-dimensional circular statistics is the von Mises distribution, which has a simpler analytic form than the wrapped normal distribution. The von Mises distribution is also normally distributed in the limit of a narrow distribution, uniform in the limit of a broad distribution, and in general a close approximation but not identical to the wrapped normal distribution. Von Mises distributions provide fits of comparable qualitative quality to $\theta(t)$ as wrapped normal distributions. For the von Mises distribution, $\frac{N}{N-1}(\bar{\rho}^2 - \frac{1}{N})$ is an unbiased maximum likelihood estimator related to the width. By the Cramér-Rao inequality, a lower mean-squared error cannot be achieved if $\theta(t)$ is von Mises. Particularly in the limit of a broad distribution where all circular distributions tend towards uniform, it would be very surprising if an estimator could be found that satisfied this bound for the von Mises case but could reliably estimate the width of $\theta(t)$ in the noise region if a different underlying distribution is assumed.

FIG. 25: The first four cumulants of $\frac{d\theta}{dt}$.FIG. 26: Histograms of $\frac{d\theta}{dt}$ with fits to a wrapped stable mixture distribution shown as the purple curves. See the main text for details.

Like $\frac{dR}{dt}$, $\frac{d\theta}{dt}$ shows evidence of heavy tails. The time evolution of $R(t)$ and $\theta(t)$ for three (randomly selected) correlation functions are shown in Fig. 28, and exhibit large jumps in both $R(t)$ and $\theta(t)$ more characteristic of Lévy flights than Brownian motion, leading us to consider stable distributions once again. Wrapped stable distributions can be constructed analogously to wrapped normal distributions as

$$\begin{aligned} \mathcal{P}_{WS}(\theta; \alpha, \beta, \mu, \gamma) &= \sum_{k=-\infty}^{\infty} \mathcal{P}_S(\theta + 2\pi k; \alpha, \beta, \mu, \gamma) \\ &= \frac{1}{2\pi} \sum_{n=-\infty}^{\infty} \exp \left(i\mu n - |\gamma n|^\alpha \left[1 - i\beta \frac{n}{|n|} \tan(\pi\alpha/2) \right] \right) \quad , \end{aligned} \quad (37)$$

where, as in Eq. (21), $\tan(\pi\alpha/2)$ should be replaced by $-\frac{2}{\alpha} \ln|n|$ for $\alpha = 1$. This wrapped stable distribution is still not appropriate to describe $\frac{d\theta}{dt}$ for two reasons. First, $\frac{d\theta}{dt}$ describes a difference of angles and so is defined on a periodic domain $-2\pi < \frac{d\theta}{dt} \leq 2\pi$. This is trivially accounted for by replacing 2π by 4π in Eq. (37). Second, $\theta(t)$ is determined from a complex logarithm of $C(t)$ with a branch cut placed at $\pm\pi$. Whenever $\theta(t)$ makes a small jump across this branch cut, $\frac{d\theta}{dt}$ will be measured to be around 2π even though the distance traveled by $\theta(t)$ along its full Riemann surface is much smaller. This behavior results in the small secondary peaks near $\frac{d\theta}{dt} = \pm 2\pi$ visible in Fig. 26. This can be accommodated by fitting $\frac{d\theta}{dt}$ to a mixture of wrapped stable distributions peaked at zero and 2π . Since $\theta(t) \rightarrow -\theta(t)$ symmetry demands that both of these distributions are symmetric, a probability distribution able to accommodate all observed features of $\frac{d\theta}{dt}$ is given by the wrapped stable mixture distribution

$$\tilde{\mathcal{P}}_{WS}(\theta; \alpha_1, \alpha_2, \gamma_1, \gamma_2, f) = \frac{1}{4\pi} \left[1 + 2 \sum_{n=1}^{\infty} (1-f) e^{-|\gamma_1 n|^{\alpha_1}} \cos(n\theta) + f e^{-|\gamma_2 n|^{\alpha_2}} \cos(n(\theta - 2\pi)) \right] \quad , \quad (38)$$

where f represents the fraction of $\frac{d\theta}{dt}$ data in the secondary peaks at $\frac{d\theta}{dt} = \pm 2\pi$ representing branch cut crossings. Fits of $\frac{d\theta}{dt}$ to this wrapped stable mixture model performed with maximum likelihood estimation are shown in Fig. 26 and are in good qualitative agreement with the LQCD results.

If the widths of the main and secondary peaks in $\frac{d\theta}{dt}$ were sufficiently narrow, it would be possible to unambiguously associate each $\frac{d\theta}{dt}$ measurement with one peak or the other and “unwrap” the trajectory of $\theta(t)$ across its full Riemann

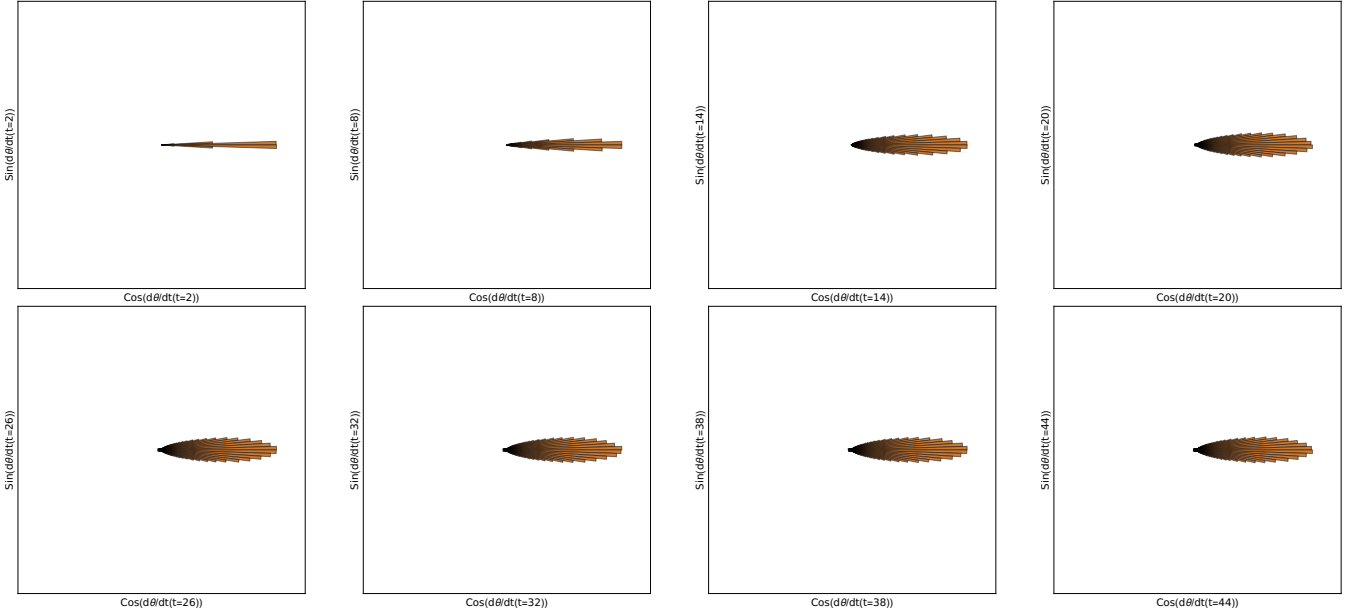


FIG. 27: Angular histograms of $\frac{d\theta}{dt}$. Since $\frac{d\theta}{dt}$ is defined on $-2\pi < \frac{d\theta}{dt} \leq 2\pi$, normalizations are such that $\frac{1}{2} \frac{d\theta}{dt}$ is mapped to the unit circle in analogy to Fig. 21.

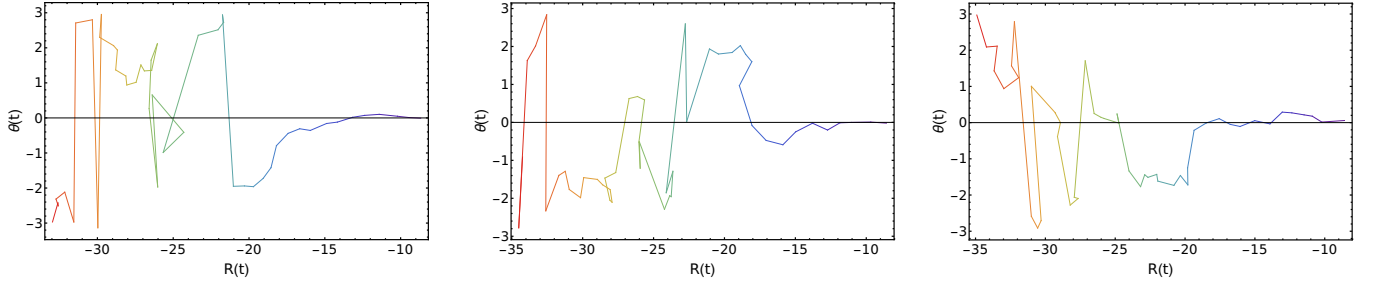


FIG. 28: Time series showing $R(t)$ on the horizontal axis and $\theta(t)$ on the vertical axis for three individual nucleon correlation functions, where the color of the line shows the time evolution from violet at $t = 0$ to red at $t = 48$. The evolution of $R(t)$ shows a clear drift towards increasingly negative $R(t)$. The middle and right panels show large jumps where $\theta(t)$ changes by nearly $\pm 2\pi$, which likely correspond to crossing a branch cut. There are also sizable jumps where $\theta(t)$ changes by nearly $\pm\pi$ which likely do not correspond to crossing a branch cut.

surface by adding $\pm 2\pi$ to measured values of $\frac{d\theta}{dt}$ whenever the branch cut in $\theta(t)$ is crossed. This should become increasingly feasible as the continuum limit is approached. However, the presence of heavy tails in the $\frac{d\theta}{dt}$ primary peak prevent unambiguous identification of branch cut crossings in the LQCD correlation functions considered here. Due to the power-law decay of the primary peak, there is no clear separation visible between the main and secondary peaks, and in particular, points near $\frac{d\theta}{dt} = \pm\pi$ cannot be unambiguously identified with one peak or another.

For descriptive analysis of $\frac{d\theta}{dt}$, it is useful to shift the secondary peak to the origin by defining

$$\widetilde{\Delta\theta} = \text{Mod}(\Delta\theta + \pi, 2\pi) - \pi \quad . \quad (39)$$

$\widetilde{\Delta\theta}$ is well-described by the wrapped stable distribution of Eq. (37). Histograms of the late-time behavior of $\widetilde{\Delta\theta}$ are shown in Fig. 29 for $\Delta t = 4, 8$ and fits of the index of stability of $\widetilde{\Delta\theta}$ are shown in Fig. 30. The late-time distribution of $\widetilde{\Delta\theta}(t, \Delta t)$ appears time independent for all Δt . Heavy tails are visible at all times, even as Δt becomes large. The large Δt behavior visible here is consistent with a wrapped Cauchy distribution. The estimated index of stability of $\widetilde{\Delta\theta}$ differs significantly from that of ΔR , and for $\Delta t = 1$, the late-time behavior is found to have

$$\alpha(\widetilde{\Delta\theta}(t \rightarrow \infty, \Delta t \sim 0.12 \text{ fm})) \rightarrow 1.267(4)(1) \quad . \quad (40)$$

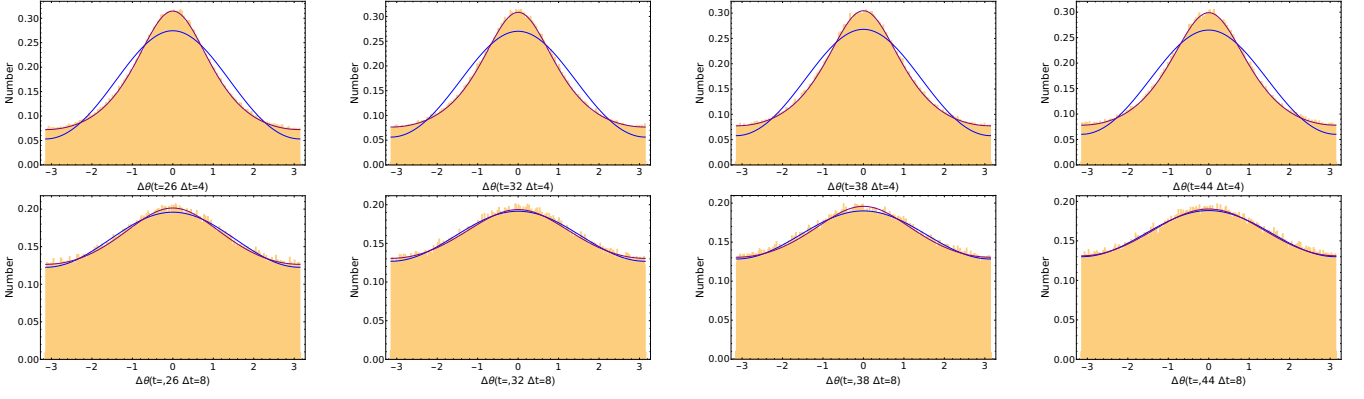


FIG. 29: Histograms of $\widetilde{\Delta\theta}$ along with fits to wrapped normal distributions in blue and wrapped stable distributions in purple.

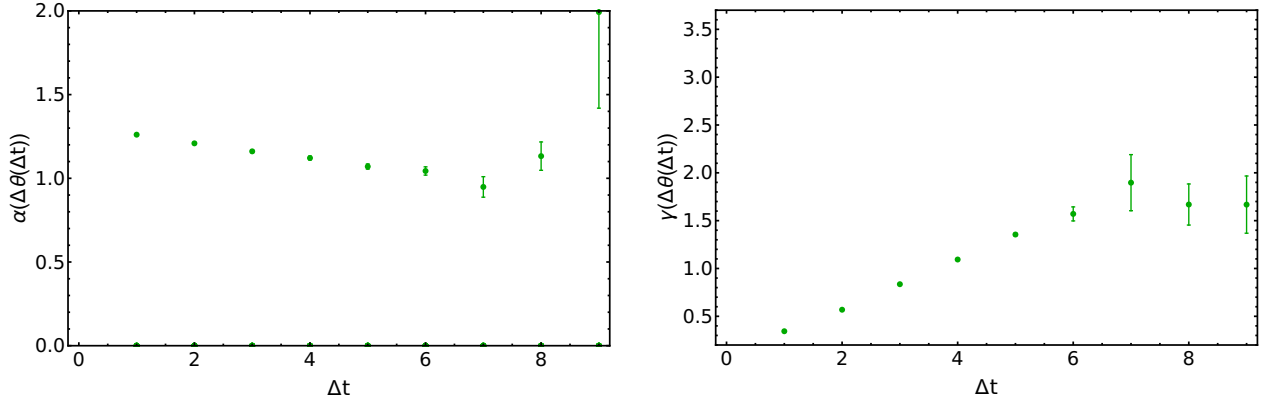


FIG. 30: Maximum likelihood estimates for the wrapped stable index of stability $\alpha(\widetilde{\Delta\theta})$, left, and width $\gamma(\widetilde{\Delta\theta})$, right extracted from the late time plateau region as functions of Δt .

This result is consistent with maximum likelihood estimates of $\alpha_1(\frac{d\theta}{dt})$ in the wrapped stable mixture model of Eq. (38). $\alpha_2(\frac{d\theta}{dt})$, associated with the peak shifted from $\theta = \pm\pi$ in the wrapped stable mixture model, cannot be reliably estimated from the available LQCD correlation functions. The continuum limit index of stability of $\frac{d\theta}{dt}$ cannot be determined without additional LQCD studies at finer lattice spacings.

As seen in Fig. 30, the late-time width of $\widetilde{\Delta\theta}(t, \Delta t)$ increases with increasing Δt . This behavior is shared by $\Delta\theta(t, \Delta t)$. In accordance with the observations above that the wrapped normal variance of $\theta(t)$ increases linearly with t , the constant late-time wrapped normal variance of $\Delta\theta(t, \Delta t)$ increases linearly with Δt . This is consistent with a picture of $\Delta\theta(t, \Delta t)$ as the sum of Δt single time step differences, $\frac{d\theta}{dt}$, that make roughly equal contributions to $\Delta\theta(t, \Delta t)$. In accordance with the scaling $\sigma^2(\theta(t)) \sim (m_N - \frac{3}{2}m_\pi)t$ discussed previously, this linear scaling gives $\sigma^2(\Delta\theta(t, \Delta t)) \sim 2(m_N - \frac{3}{2}m_\pi)\Delta t$.

We summarize our observations on the phase of $C(t)$:

- The phase of the nucleon correlation function is described by an approximately wrapped normal distribution whose width increases with time. At early times the distribution is narrow and resembles a normal distribution. At late times the distribution becomes broad compared to the 2π range of definition of $\theta(t)$ and resembles a uniform distribution.
- The phase effective mass $m_\theta(t)$ appears to plateau to a value close to $m_N - 3/2m_\pi$. Since $|e^{i\theta(t)}|^2 = 1$ is time-independent by construction, this non-zero asymptotic value of m_θ implies $\theta(t)$ has a severe StN problem.
- $m_\theta(t)$ can be determined from the time derivative of the wrapped normal variance of $\theta(t)$ in analogy to the cumulant expansion. The effective mass extracted from growth of the wrapped normal variance is identical to $m_\theta(t)$ up to statistical fluctuations. This leads to scaling of the wrapped normal variance of $\theta(t)$ consistent with $\sigma^2(\theta(t)) \sim 2(m_N - \frac{3}{2}m_\pi)t$.

- Standard estimators for the wrapped normal variance have a systematic bias and for a sufficiently broad distribution the minimum expected statistical uncertainty is set by finite sample size $1/N$ effects. Once the wrapped normal variance becomes larger than $\ln N$, finite sample size fluctuations become larger than the signal required to extract $m_\theta(t)$. Since the width of $\theta(t)$ increases with time, a region where finite sample size errors prevent reliable extractions of $m_\theta(t)$ will inevitably occur at sufficiently late times. This is the noise region empirically identified above. Standard effective mass estimates are systematically biased in the noise region. Exponentially large increases in statistics are necessary to delay the onset of the noise region.
- Finite differences, $\Delta\theta(t, \Delta t)$, are described by time-independent distributions at late times. $\Delta\theta$ is heavy-tailed for all Δt considered here, and $\frac{d\theta}{dt}$ is well-described by a wrapped stable mixture distribution. Further studies will be needed to understand the continuum limit of the index of stability of $\frac{d\theta}{dt}$.

IV. AN IMPROVED ESTIMATOR

The proceeding observations suggest that difficulties in statistical analysis of nucleon correlation functions arise from difficulties in statistical inference of $\theta(t)$. The same exponentially hard StN and noise region problems obstruct late-time estimation of the wrapped normal variance of $\theta(t)$ and of $m(t)$. Conversely, the width of $\Delta\theta(t, \Delta t)$ distributions does not increase with time, and there is no StN problem impeding statistical inference of $\Delta\theta(t, \Delta t)$. This suggests that it would be preferable to construct an effective mass estimator relying on statistical inference of $\Delta\theta(t, \Delta t)$.

First consider the log-magnitude for simplicity. The mean correlation function magnitude can be expressed in terms of ΔR as

$$\begin{aligned} \langle e^{R(t)} \rangle &= \left\langle \exp \left(R(0) + \sum_{t'=1}^t \frac{dR}{dt} \Big|_{t'} \right) \right\rangle \\ &= \left\langle \exp \left(R(0) + \sum_{t'=1}^{t-\Delta t} \frac{dR}{dt} \Big|_{t'} \right) \exp \left(\sum_{t'=t-\Delta t+1}^t \frac{dR}{dt} \Big|_{t'} \right) \right\rangle \\ &= \left\langle e^{R(0)+\Delta R(t-\Delta t, t-\Delta t)} e^{\Delta R(t, \Delta t)} \right\rangle. \end{aligned} \quad (41)$$

The last expression above shows that $e^{R(t)}$ can be expressed as a product of two factors involving the evolution of $R(t)$ in the regions $[0, t-\Delta t]$ and $[t-\Delta t, t]$ respectively. Because QCD has a finite correlation length, these two factors should be approximately decorrelated. Correlations should only arise from contributions involving points near the boundary at $t-\Delta t$. At late times, t can be assumed to be much larger than Δt and than any QCD correlation length, so boundary effects can be assumed to be negligible for the first region. Boundary effects cannot be neglected for the shorter region of length Δt . As t and Δt are increased with $t \gg \Delta t \gg m_\pi^{-1}$, systematic uncertainties introduced by neglecting the correlations between the regions $[0, t-\Delta t]$ and $[t-\Delta t, t]$ are expected to be parametrically suppressed by $e^{-m_\pi \Delta t}$. Eq. (41) can therefore be expressed as an uncorrelated product plus a parametrically suppressed systematic error term,

$$\langle e^{R(t)} \rangle = \langle e^{R(0)+\Delta R(t-\Delta t, t-\Delta t)} \rangle \langle e^{\Delta R(t, \Delta t)} \rangle + O(e^{-m_\pi \Delta t}). \quad (42)$$

$e^{R(t+1)}$ can similarly be split into an approximately decorrelated product. Performing this split with regions $[0, t-\Delta t]$ and $[t-\Delta t, t+1]$ gives

$$\langle e^{R(t+1)} \rangle = \langle e^{R(0)+\Delta R(t-\Delta t, t-\Delta t)} \rangle \langle e^{\Delta R(t+1, \Delta t+1)} \rangle + O(e^{-m_\pi \Delta t}). \quad (43)$$

The common term in both expressions cancels when constructing the magnitude effective mass, leaving

$$m_R(t) = \ln \left[\frac{\langle e^{\Delta R(t, \Delta t)} \rangle}{\langle e^{\Delta R(t+1, \Delta t+1)} \rangle} \right] + O(e^{-m_\pi \Delta t}). \quad (44)$$

Identical steps can be applied to the phase, leading to

$$m_\theta(t) = \ln \left[\frac{\langle e^{i\Delta\theta(t, \Delta t)} \rangle}{\langle e^{i\Delta\theta(t+1, \Delta t+1)} \rangle} \right] + O(e^{-m_\pi \Delta t}). \quad (45)$$

Further, the same steps can also be applied to the full correlation function $C(t) = e^{R(t)+i\theta(t)}$. Noting that

$$e^{\Delta R(t,\Delta t)+i\Delta\theta(t,\Delta t)} = \frac{C(t)}{C(t-\Delta t)} \quad , \quad (46)$$

the analogous relation for the full effective mass takes the simple form

$$m(t) = \ln \left[\frac{\langle C(t)/C(t-\Delta t) \rangle}{\langle C(t+1)/C(t-\Delta t) \rangle} \right] + O(e^{-m_\pi \Delta t}) \quad . \quad (47)$$

Neglecting the $O(e^{-m_\pi \Delta t})$ terms on the right-hand-sides of Eq. (44), Eq. (45), and Eq. (47) gives estimators for the magnitude, phase, and full effective mass that we will denote $m_R(t, \Delta t)$, $m_\theta(t, \Delta t)$, and $m(t, \Delta t)$ respectively. The usual sample mean effective mass estimators are recovered as the special case $\Delta t = t$ of these estimators. As described below, taking Δt to be a fixed length much less than t makes $m(t, \Delta t)$ an improved estimator for the nucleon mass with a systematically reducible bias of order $e^{-m_\pi \Delta t}$ and greatly improved statistical behavior.

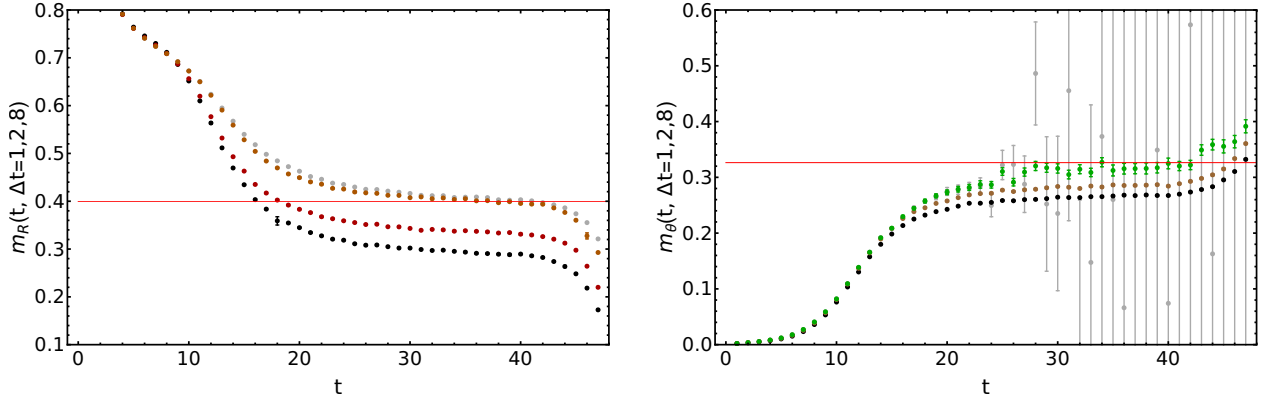


FIG. 31: Results for the improved estimators $m_R(t, \Delta t)$ and $m_\theta(t, \Delta t)$ with $\Delta t = 1, 2, 8$. The left panel shows results for $m_R(t, \Delta t)$ with $\Delta t = 1$ in black, $\Delta t = 2$ in red, and $\Delta t = 8$ in orange. The standard estimator $m_R(t)$ is shown in gray, and a red line is shown for reference at $\frac{3}{2}m_\pi$. The right panel shows results for $m_\theta(t, \Delta t)$ with $\Delta t = 1$ in black, $\Delta t = 2$ in brown, and $\Delta t = 8$ in green. The standard estimator $m_\theta(t)$ is shown in gray and a red line is shown for reference at $m_N - \frac{3}{2}m_\pi$.

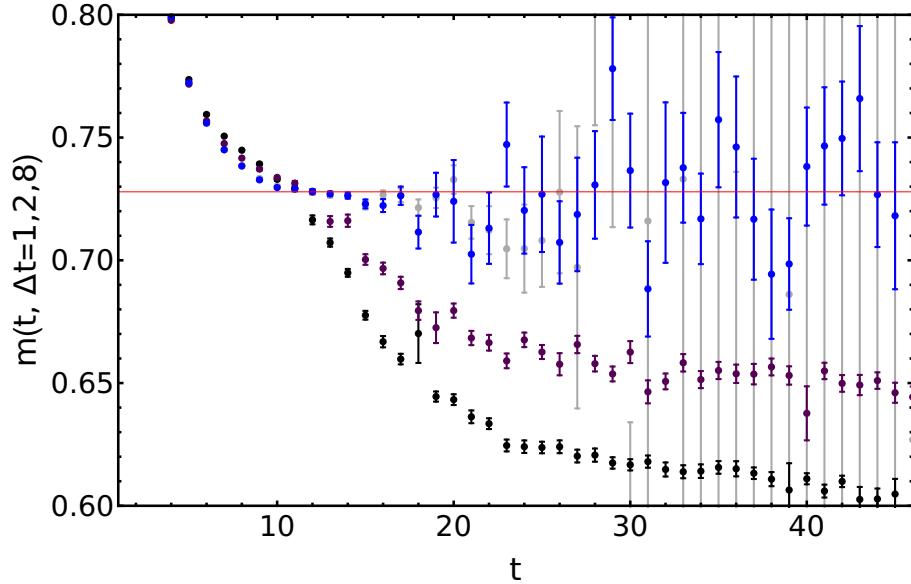


FIG. 32: Results for the improved estimator $m(t, \Delta t)$. The left panel shows results with $\Delta t = 1$ in black, $\Delta t = 2$ in purple, and $\Delta t = 8$ in blue, along with the standard estimator $m(t)$ shown in gray and a red line at m_N shown for reference.

The LQCD results for $m_R(t, \Delta t)$ and $m_\theta(t, \Delta t)$ with $\Delta t = 1, 2, 8$ are shown in Fig. 31, and results for $m(t, \Delta t)$ are shown in Fig. 32. The statistical uncertainties associated with $m(t, \Delta t)$ are the same as those of $m(t)$ within the golden window, but at late times they become constant in time rather than exponentially increasing. This is in accord with our observations about the form of the statistical distributions associated with $\Delta R(t, \Delta t)$ and $\Delta \theta(t, \Delta t)$, which, up to small magnitude-phase correlations, indicate that

$$\text{Var}(m(t, \Delta t)) \sim \frac{\text{Var}(e^{R(t, \Delta t) + i\theta(t, \Delta t)})}{\langle e^{R(t, \Delta t) + i\theta(t, \Delta t)} \rangle^2} \sim e^{2(m_N - \frac{3}{2}m_\pi)\Delta t} \quad (48)$$

The statistical uncertainties associated with $m(t, \Delta t)$ are constant in t , although they do increase exponentially with increases in Δt . Since $\Delta \theta(t, \Delta t)$ has constant width at late times, the inevitable onset of the noise region where statistical inference fails for $\theta(t)$ can be avoided. The constraint required for reliable statistical inference of $m(t, \Delta t)$ at late times is that the wrapped normal variance of $\Delta \theta(t, \Delta t)$ can be extracted without large finite sample size errors. This constraint can be expressed as a bound on the statistical sample size required for a particular choice of Δt ,

$$N > e^{\sigma^2(\Delta \theta(t, \Delta t))} \sim e^{2(m_N - \frac{3}{2}m_\pi)\Delta t} \quad (49)$$

The statistical uncertainties of $m(t, \Delta t)$ determined from the LQCD correlation functions are shown in Fig. 33, from which it can be seen that they become constant at late times for all fixed Δt . For small and moderately large values of $\Delta t = 1, 7, 15$, the expected exponential increase in late-time statistical uncertainties is observed, consistent with Eq. (49). Once Eq. (49) is violated, exponential scaling of statistical uncertainties with Δt ceases. For $\Delta t > \frac{\ln(N)}{2(m_N - \frac{3}{2}m_\pi)}$, the relative statistical uncertainty in $m(t, \Delta t)$ compared to $m(t, \Delta t = 1)$ is equal to N rather than $e^{2(m_N - \frac{3}{2}m_\pi)(\Delta t - 1)}$. This is seen in Fig. 33 in the late-time behavior of the standard effective mass.

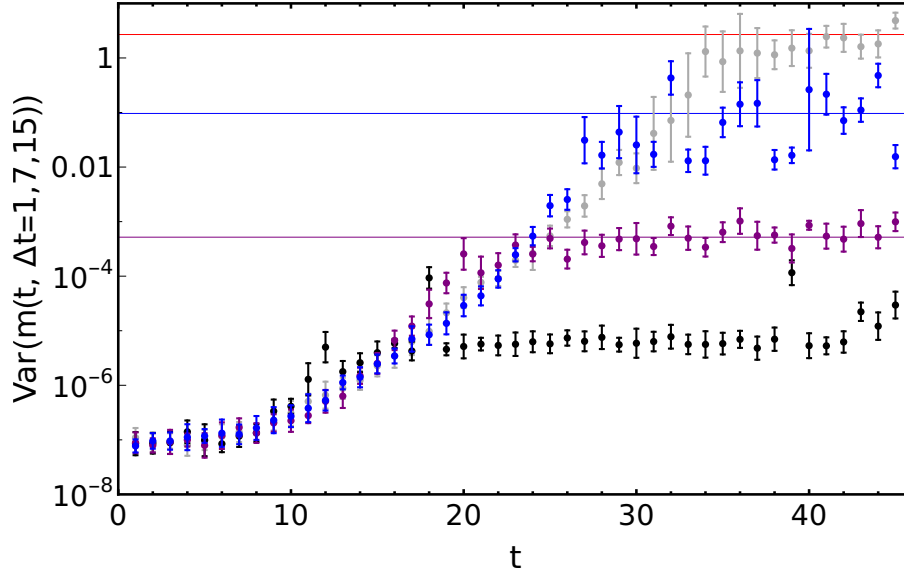


FIG. 33: Variance in the estimates of $m(t, \Delta t)$ as a function of time t for various choices of Δt . The black points show $\Delta t = 1$, the purple show $\Delta t = 7$, and the blue show $\Delta t = 15$. The gray points show uncertainties in the standard effective mass estimator equivalent to $\Delta t = t$. The purple and blue lines show the expected late-time variance of $m(t, \Delta t)$ with $\Delta t = 7, 15$ predicted by Eq. (48) with the overall normalization fixed by the $\Delta t = 1$ case. The red line shows the bound of Eq. (33) with overall normalization again fixed by the $\Delta t = 1$ case. Breakdown of statistical inference of broad circular distributions predicts that the late-time variance of $m(t, \Delta t)$ will not systematically rise above the red line for any Δt .

When Eq. (49) is violated, $\Delta \theta(t, \Delta t)$ cannot be reliably estimated at late times and increasing Δt does not improve the accuracy of $m(t, \Delta t)$. In particular, the standard effective mass estimator with $\Delta t = t$ is no more reliable than $m(t, \Delta t)$ with $\Delta t = \frac{\ln(N)}{2(m_N - \frac{3}{2}m_\pi)}$. The bias associated with neglected correlations in $m(t, \Delta t)$ is less important than the intrinsic bias associated with statistical inference of overly broad circular random variables. In practice, exponential growth of statistical uncertainties with Δt suggests that smaller choices of Δt , where Eq. (49) holds, likely lead to smaller overall statistical plus systematic uncertainties.

The systematic bias of $m(t, \Delta t)$ can be explored through calculations at various Δt . Fig. 34 shows results for with $\Delta t = 1, \dots, 9$. For $\Delta t \gtrsim 4$, results for $m(t, \Delta t)$ fit during the late-time noise region $25 \leq t \leq 40$ are statistically consistent with fits extracted from the golden window $15 \leq t \leq 25$. Late-time fits with $m(t, \Delta t)$ have larger statistical uncertainties than golden window fits. More precise fits than either could be made by including both the golden window and the noise region in fits of $m(t, \Delta t)$. There is only a minor advantage in including the noisier late-time points in fits that include a precise golden window, and this exploratory work does not aim for a more precise extraction of the nucleon mass. Practical advantages of late-time fits of $m(t, \Delta t)$ compared to golden window fits of $m(t)$ are more likely to be found in systems where a reliable golden window cannot be unambiguously identified. Late-time fits of $m(t, \Delta t)$ would also be more advantageous with longer time directions where there is a larger late-time region.

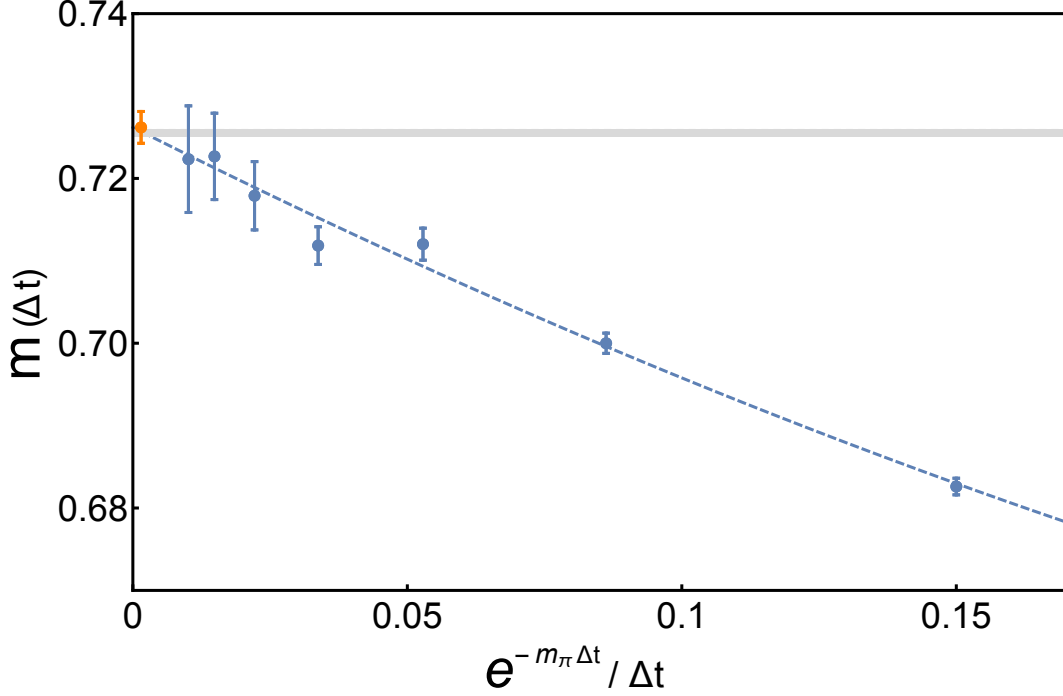


FIG. 34: Results for $m(\Delta t)$ with $\Delta t = 3, \dots, 9$ shown as the blue points. The $m(\Delta t)$ are extracted from constant fits to plateaus in the late-time noise region $25 \leq t \leq 40$, where standard estimators of the effective mass are unreliable. The light blue curve shows the best fit to Eq. (50) used to estimate and remove the systematic bias of $m(t, \Delta t)$, and the orange point shows the extrapolation to $\Delta t = \infty$. The horizontal gray line shows the value of m_N extracted from the golden window.

Results including various Δt shown in Fig. 34 can also be used to fit the systematic bias of $m(t, \Delta t)$ and formally extrapolate to the unbiased $\Delta t \rightarrow \infty$ result. Performing a fit of $m(\Delta t)$ (obtained from late time fits to $m(t, \Delta t)$) to large Δt , $\Delta t \geq 3$, to a form motivated by the corrections to the mass of the nucleon in a finite spatial volume, [43]

$$m(\Delta t) = m_N^\infty + c \frac{e^{-m_\pi \Delta t}}{\Delta t} + \dots, \quad (50)$$

where c is a constant, gives results

$$m_N^\infty = 0.7259(15) \quad \text{and} \quad c = -0.354(22), \quad (51)$$

where a small quadratic term has been included in the fit also. The extracted value of the nucleon mass from the noise region using the new estimator in Eq. (47) is observed to be in good agreement with the precision extraction from the golden window.

The improved estimator proposed here exploits physical locality and finite correlation lengths to extract the effective mass from the evolution of $C(t)$ between times $t - \Delta t$ and t rather than the full evolution between source time $t = 0$ and sink time t . The correlation function at time $t - \Delta t$ is effectively treated as a new source so that the effective source/sink separation is fixed to be a constant length Δt rather than an increasing separation t . The effective source at $t - \Delta t$ still incorporates the dynamical evolution of the system between time 0 and $t - \Delta t$, and in particular has exponentially reduced excited state contamination compared to the original source. In principle t can be taken arbitrarily large

with Δt fixed in order to extract a plateau in $m(t, \Delta t)$ with arbitrarily small excited state contamination and constant statistical uncertainties across the plateau. The length of the lattice time direction becomes the only factor limiting the length of the plateau in this case.

Similar physical ideas underlie the hierarchical integration approach of Ref. [44]. In that approach, locality is exploited to decompose correlation functions into products of factors that can be computed on subsets of a lattice volume with exponentially reduced StN problems. Hierarchical integration has been successfully implemented in studies of gluonic observables [45–49] and recently explored for baryon correlation functions in the quenched approximation [50] and beyond [51]. For baryon correlators, the method of Ref. [50] implements approximate factorization with systematically reducible uncertainties, as in the method proposed here. However, the method proposed here provides two major advantages over hierarchical integration. First, exponential growth of uncertainties is entirely removed at late times rather than slowed. Second, hierarchical integration requires modified MC integration with additional updates of sub-lattice observables, while the method proposed here applies to correlation function computed with standard MC methods and introduces no additional cost or modification to generation of LQCD gauge ensembles. In addition, it also has similarities to the generalized pencil-of-functions method introduced to LQCD in Ref. [52], where correlation functions involving shifted source and sink times are combined in a variational basis. In the generalized pencil-of-functions approach, shifted source and sink times have primarily been investigated to reduce excited-state contamination rather than StN improvement.

In some sense, Δt can be considered a “factorization” scale in the time direction. The LQCD calculations are valid for all energy scales below that defined by the inverse lattice spacing, π/a . While well-defined, the MC sampling of the path integral and analysis of baryon correlation functions fails to converge in the noise region because of the quantum fluctuations encountered along the paths from the source to late times, which include many incoherent hadronic volumes. The new estimator provides exponentially-improved signal extraction at late times through limiting the number of contributing hadronic volumes to those within Δt , but does not provide a complete description of the IR behavior of QCD, introducing a bias in the extracted mass of the nucleon. An extrapolation in Δt , using a form motivated by low-energy pion physics, is used to remove this bias. While different, this reminds one of matching LQCD calculations to the p-regime of chiral perturbation theory to remove finite-spatial-volume effects. The idea of performing an extrapolation to overcome a sign problem is not new. It was introduced thirty years ago to deal with the sign problem in MC calculations of modest size nuclei [53], and recently used in lattice effective field theory calculations to continuously evolve between the eigenvalues of nuclear many-body systems described by a Hamiltonian without a sign problem to one that does have a sign problem [54].

V. SUMMARY AND CONCLUSIONS

This work presents observations about the nucleon correlation function in LQCD that highlight the role of the complex phase in the signal-to-noise problem. The magnitude is found to have no StN problem and has the late-time scaling $\langle |C(t)| \rangle \sim e^{-\frac{3}{2}m_\pi t}$. The nucleon log-magnitude, $R(t)$, is approximately described by a normal distribution with linearly increasing mean and almost constant variance. The complex phase, which gives the direct importance sampling of $C(t)$ a sign problem, has the late-time scaling of approximately $\langle e^{i\theta(t)} \rangle \sim e^{-(m_N - \frac{3}{2}m_\pi)t}$. The StN problem arising from reweighting the complex phase of the nucleon correlation function matches the nucleon StN problem.

We present evidence that nucleon correlation functions are statistically described by a nearly decorrelated product of an approximately log-normal magnitude and wrapped normal phase. Log-normal times wrapped normal complex correlation functions are consistent with the arguments of Endres, Kaplan, Lee, and Nicholson [13], who suggested stable distributed correlation function logarithms may be a generic feature of quantum field theory and pursued a systematic statistical analysis of unitary fermion correlation functions that provides inspiration for this work. The wrapped normal phase distribution broadens with time, and at late-times cannot be reliably distinguished from a uniform distribution. A noise region begins at this point where the sample mean phase becomes biased and systematically deviates from the true mean phase. In contrast, and importantly, $\frac{dR}{dt}$ and $\frac{d\theta}{dt}$ are described by approximately stable and wrapped stable distributions respectively that become constant at late times and can be estimated in the noise region with no StN problem.

It is remarkable that the Euclidean-time derivate of the logarithm of the correlation function is described by a heavy-tailed distribution while the logarithm itself is nearly normally distributed at all times. Further studies will be needed to understand the dynamical origin, continuum limit behavior, and universality of heavy-tailed Euclidean-time evolution of correlation functions in quantum field theory. LQCD calculations at finer lattice spacings are needed to explore the continuum limit of the index of stability describing time evolution of the nucleon correlation function. Perturbative QCD and model calculations will provide useful insights into the dynamical origin of heavy-tailed time evolution of the nucleon correlation function. Lattice and continuum studies of other quantum field theories are required to understand the universality of heavy-tailed Euclidean-time evolution of correlation functions. Implications

for real-time evolution are also left for future investigations.

Building on the observation that $\frac{d\theta}{dt}$ has constant width at late times, we have proposed a new estimator in Eq. (47) for the effective mass of the nucleon correlation function that relies on statistically sampling ratios of correlation functions at different times. At asymptotically large times, this estimator has statistical uncertainties that are constant in time and therefore has no StN problem. This estimator has a systematic bias arising from factorizing correlation functions into approximately decorrelated products of terms involving regions $[0, t - \Delta t]$ and $[\Delta t, t]$ respectively. For $\Delta t > \frac{\ln(N)}{2(m_N - \frac{3}{2}m_\pi)}$, this systematic bias is dominated by that associated with statistical inference of circular random variables that also affects standard estimators in the noise region. As Δt is increased, the systematic bias decreases as (for light quarks) $e^{-m_\pi \Delta t}$, while the statistical uncertainty increases as $e^{2(m_N - \frac{3}{2}m_\pi)\Delta t}$. Moderate values of Δt can be chosen to minimize the combined statistical and systematic uncertainties. It is also possible to fit and remove the $e^{-m_\pi \Delta t}$ systematic uncertainty by calculating $m(t, \Delta t)$ over a range of Δt .

The properties of the new estimator that we have introduced may prove advantageous in the analysis of LQCD calculations of nuclei. Such systems are plagued by a reduced golden window compared to the single nucleon, presently limiting the length of plateaus from which to extract energy eigenvalues. A re-analysis of existing nuclear correlation functions generated by the NPLQCD collaboration [24, 55, 56] is planned in order to determine the utility of this work for such systems. Binding momenta and other scales appearing in multi-body hadronic systems may affect the form of the extrapolation used to remove the bias of the new estimator. It will be important to verify and further understand the scaling of the new estimator with pion mass and lattice spacing, as well as to investigate dependences on smearing scales and other scales appearing in LQCD calculations. Studies of the vacuum channel including glueballs and scalar mesons and analyses of disconnected diagrams provide additional directions for further studies. Forming ratios of position space, rather than momentum space, correlation functions may be advantageous in future studies. Other types of LQCD calculations may also benefit from the new estimator, for instance in the isoscalar meson sector and those at non-zero baryon chemical potential.

It is not expected that the statistical properties of $\theta(t)$ discussed here and, in particular the constant late-time width of $\frac{d\theta}{dt}$, are unique to single-nucleon correlation functions. If analogous statistical properties apply to generic complex correlation functions in quantum field theory, then estimators analogous to Eq. (47) can be constructed to extract the spectra of complex correlation functions and reweighted complex actions without StN problems. It will be interesting to learn if the approaches developed in this work can be fruitfully applied to other systems in particle, nuclear, and condensed matter physics that encounter sign and StN problems.

Acknowledgments: We would like to thank David Kaplan, Natalie Klco, Silas Beane, Emmanuel Chang, Aleksey Cherman, Zohreh Davoudi, William Detmold, Dorota Grabowska, Kostas Orginos, Phiala Shanahan and Brian Tiburzi for interesting discussions. This research was supported in part by the National Science Foundation under grant number NSF PHY11-25915 and we acknowledge the Kavli Institute for Theoretical Physics for hospitality during much of this work. Much of the post-production analysis of the nucleon correlation functions for this project was carried out on the Hyak High Performance Computing and Data Ecosystem at the University of Washington, supported, in part, by the U.S. National Science Foundation Major Research Instrumentation Award, Grant Number 0922770, and by the UW Student Technology Fee (STF). Calculations were performed using computational resources provided by NERSC (supported by U.S. Department of Energy grant number DE-AC02-05CH11231), and by the USQCD collaboration. This research used resources of the Oak Ridge Leadership Computing Facility at the Oak Ridge National Laboratory, which is supported by the Office of Science of the U.S. Department of Energy under Contract number DE-AC05-00OR22725. The PRACE Research Infrastructure resources at the Très Grand Centre de Calcul and Barcelona Supercomputing Center were also used. Parts of the calculations used the Chroma software suite [57]. MJS was supported by DOE grant number DE-FG02-00ER41132, and in part by the USQCD SciDAC project, the U.S. Department of Energy through grant number DE-SC00-10337. MLW was supported in part by DOE grant number DE-FG02-00ER41132.

-
- [1] G. Parisi, Phys. Rept. **103**, 203 (1984).
 - [2] G. P. Lepage, in *Boulder ASI 1989:97-120* (1989), pp. 97–120, URL <http://alice.cern.ch/format/showfull?sysnb=0117836>.
 - [3] C. Bernard and M. Golterman, Phys. Rev. **D88**, 014004 (2013), 1304.1948.
 - [4] D. Weingarten, Phys. Rev. Lett. **51**, 1830 (1983).
 - [5] E. Witten, Phys. Rev. Lett. **51**, 2351 (1983).
 - [6] W. Detmold, Phys. Rev. Lett. **114**, 222001 (2015), 1408.6919.

- [7] S. R. Beane, W. Detmold, T. C. Luu, K. Orginos, A. Parreno, M. J. Savage, A. Torok, and A. Walker-Loud, Phys. Rev. **D79**, 114502 (2009), 0903.2990.
- [8] S. R. Beane, W. Detmold, K. Orginos, and M. J. Savage, Prog. Part. Nucl. Phys. **66**, 1 (2011), 1004.2935.
- [9] S. R. Beane, W. Detmold, K. Orginos, and M. J. Savage, J. Phys. **G42**, 034022 (2015), 1410.2937.
- [10] W. Detmold and M. G. Endres, PoS **LATTICE2014**, 170 (2015), 1409.5667.
- [11] W. Detmold and M. G. Endres, Phys. Rev. **D90**, 034503 (2014), 1404.6816.
- [12] M. J. Savage (2010).
- [13] M. G. Endres, D. B. Kaplan, J.-W. Lee, and A. N. Nicholson, Phys. Rev. Lett. **107**, 201601 (2011), 1106.0073.
- [14] M. G. Endres, D. B. Kaplan, J.-W. Lee, and A. N. Nicholson, Phys. Rev. **A84**, 043644 (2011), 1106.5725.
- [15] M. G. Endres, D. B. Kaplan, J.-W. Lee, and A. N. Nicholson, PoS **LATTICE2011**, 017 (2011), 1112.4023.
- [16] J.-W. Lee, M. G. Endres, D. B. Kaplan, and A. N. Nicholson, PoS **LATTICE2011**, 203 (2011), 1111.3793.
- [17] M. G. Endres, D. B. Kaplan, J.-W. Lee, and A. N. Nicholson, Phys. Rev. **A87**, 023615 (2013), 1203.3169.
- [18] D. Grabowska, D. B. Kaplan, and A. N. Nicholson, Phys. Rev. **D87**, 014504 (2013), 1208.5760.
- [19] A. N. Nicholson, D. Grabowska, and D. B. Kaplan (2012), [J. Phys. Conf. Ser.432,012032(2013)], 1210.7250.
- [20] T. DeGrand, Phys. Rev. **D86**, 014512 (2012), 1204.4664.
- [21] N. Fisher, *Statistical Analysis of Circular Data*, Statistical Analysis of Circular Data (Cambridge University Press, 1995), ISBN 9780521568906, URL <https://books.google.com/books?id=wGPj3EoFdJwC>.
- [22] G. Borraile, *Statistics of Earth Science Data: Their Distribution in Time, Space and Orientation* (Springer Berlin Heidelberg, 2003), ISBN 9783540436034, URL <https://books.google.com/books?id=R3GpDglV0SEC>.
- [23] K. Mardia and P. Jupp, *Directional Statistics*, Wiley Series in Probability and Statistics (Wiley, 2009), ISBN 9780470317815, URL <https://books.google.com/books?id=PTNiCm4Q-M0C>.
- [24] K. Orginos, A. Parreno, M. J. Savage, S. R. Beane, E. Chang, and W. Detmold, Phys. Rev. **D92**, 114512 (2015), 1508.07583.
- [25] M. Luscher and P. Weisz, Commun. Math. Phys. **97**, 59 (1985), [Erratum: Commun. Math. Phys.98,433(1985)].
- [26] B. Sheikholeslami and R. Wohlert, Nucl. Phys. **B259**, 572 (1985).
- [27] M. Luscher and U. Wolff, Nucl. Phys. **B339**, 222 (1990).
- [28] T. A. DeGrand and D. Toussaint, eds., *From actions to answers. Proceedings, Theoretical Advanced Study Institute in Elementary Particle Physics, Boulder, USA, June 5-30, 1989* (1990).
- [29] P. Young, *Jackknife and Bootstrap Resampling Methods in Statistical Analysis to Correct for Bias*, URL <http://young.physics.ucsc.edu/jackboot.pdf>.
- [30] T. DeGrand and D. Toussaint, eds., *From actions to answers: Theoretical Advanced Study Institute in Elementary Particle Physics* (1990).
- [31] M. Luscher, in *Modern perspectives in lattice QCD: Quantum field theory and high performance computing. Proceedings, International School, 93rd Session, Les Houches, France, August 3-28, 2009* (2010), pp. 331–399, 1002.4232, URL <https://inspirehep.net/record/846344/files/arXiv:1002.4232.pdf>.
- [32] D. Kaplan (2014), presentation entitled *Noise, Statistics and Sign Problems at Conceptual Advances in Lattice Gauge Theory (LGT14)*.
- [33] P. E. Gibbs (1986).
- [34] K. Splittorff and J. J. M. Verbaarschot, Phys. Rev. Lett. **98**, 031601 (2007), hep-lat/0609076.
- [35] K. Splittorff and J. J. M. Verbaarschot, Phys. Rev. **D75**, 116003 (2007), hep-lat/0702011.
- [36] S. R. Beane, W. Detmold, T. C. Luu, K. Orginos, A. Parreno, M. J. Savage, A. Torok, and A. Walker-Loud, Phys. Rev. **D80**, 074501 (2009), 0905.0466.
- [37] T. Iritani et al., JHEP **10**, 101 (2016), 1607.06371.
- [38] S. Chandrasekhar, Rev. Mod. Phys. **15**, 1 (1943), URL <http://link.aps.org/doi/10.1103/RevModPhys.15.1>.
- [39] J.-P. Bouchaud and A. Georges, Physics Reports **195**, 127 (1990), ISSN 0370-1573, URL <http://www.sciencedirect.com/science/article/pii/037015739090099N>.
- [40] F. Bardou, ArXiv Physics e-prints (2000), physics/0012049.
- [41] J. Voit, *The Statistical Mechanics of Financial Markets*, Texts and monographs in physics (Springer, 2005), ISBN 9783540262855, URL <https://books.google.com/books?id=V6oMS3K38BsC>.
- [42] J. P. Nolan, *Stable Distributions - Models for Heavy Tailed Data* (Birkhauser, Boston, 2015), in progress, Chapter 1 online at academic2.american.edu/~jpnolan.
- [43] M. Luscher, Commun. Math. Phys. **104**, 177 (1986).
- [44] M. Luscher and P. Weisz, JHEP **09**, 010 (2001), hep-lat/0108014.
- [45] H. B. Meyer, JHEP **01**, 048 (2003), hep-lat/0209145.
- [46] M. Della Morte and L. Giusti, Comput. Phys. Commun. **180**, 813 (2009).
- [47] M. Della Morte and L. Giusti, Comput. Phys. Commun. **180**, 819 (2009), 0806.2601.
- [48] M. Della Morte and L. Giusti, JHEP **05**, 056 (2011), 1012.2562.
- [49] M. García Vera and S. Schaefer, Phys. Rev. **D93**, 074502 (2016), 1601.07155.
- [50] M. Cè, L. Giusti, and S. Schaefer, Phys. Rev. **D93**, 094507 (2016), 1601.04587.
- [51] M. Cè, L. Giusti, and S. Schaefer (2016), 1609.02419.
- [52] C. Aubin and K. Orginos, AIP Conf. Proc. **1374**, 621 (2011), 1010.0202.
- [53] Y. Alhassid, D. J. Dean, S. E. Koonin, G. Lang, and W. E. Ormand, Phys. Rev. Lett. **72**, 613 (1994), nucl-th/9310026.
- [54] T. A. Lähde, T. Luu, D. Lee, U.-G. Meißner, E. Epelbaum, H. Krebs, and G. Rupak, Eur. Phys. J. **A51**, 92 (2015), 1502.06787.
- [55] S. R. Beane, E. Chang, S. D. Cohen, W. Detmold, H. W. Lin, T. C. Luu, K. Orginos, A. Parreno, M. J. Savage, and

- A. Walker-Loud (NPLQCD), Phys. Rev. **D87**, 034506 (2013), 1206.5219.
- [56] S. R. Beane et al. (NPLQCD), Phys. Rev. **C88**, 024003 (2013), 1301.5790.
- [57] R. G. Edwards and B. Joo (SciDAC Collaboration, LHPC Collaboration, UKQCD Collaboration), Nucl.Phys.Proc.Suppl. **140**, 832 (2005), hep-lat/0409003.